Neuroscience

The potassium channel subunit $K_V1.8$ (*Kcna10*) is essential for the distinctive outwardly rectifying conductances of type I and II vestibular hair cells

Reviewed Preprint
v2 • September 4, 2024
Revised by authors

Reviewed Preprint
v1 • January 10, 2024

Hannah R Martin, Anna Lysakowski, Ruth Anne Eatock

University of Chicago, Department of Neurobiology • University of Illinois at Chicago, Department of Anatomy and Cell Biology

Abstract

In amniotes, head motions and tilt are detected by two types of vestibular hair cells (HCs) with strikingly different morphology and physiology. Mature type I HCs express a large and very unusual potassium conductance, $g_{K,L}$, which activates negative to resting potential, confers very negative resting potentials and low input resistances, and enhances an unusual non-quantal transmission from type I cells onto their calyceal afferent terminals. Following clues pointing to $K_V1.8$ (KCNA10) in the Shaker K channel family as a candidate $g_{K,L}$ subunit, we compared whole-cell voltage-dependent currents from utricular hair cells of $K_V1.8$-null mice and littermate controls. We found that $K_V1.8$ is necessary not just for $g_{K,L}$ but also for fast- inactivating and delayed rectifier currents in type II HCs, which activate positive to resting potential. The distinct properties of the three $K_V1.8$-dependent conductances may reflect different mixing with other K_V subunits that are reported to be differentially expressed in type I and II HCs. In $K_V1.8$-null HCs of both types, residual outwardly rectifying conductances include K_V7 (KCNQ) channels.

Current clamp records show that in both HC types, $K_V1.8$-dependent conductances increase the speed and damping of voltage responses. Features that speed up vestibular receptor potentials and non-quantal afferent transmission may have helped stabilize locomotion as tetrapods moved from water to land.

Graphical abstract

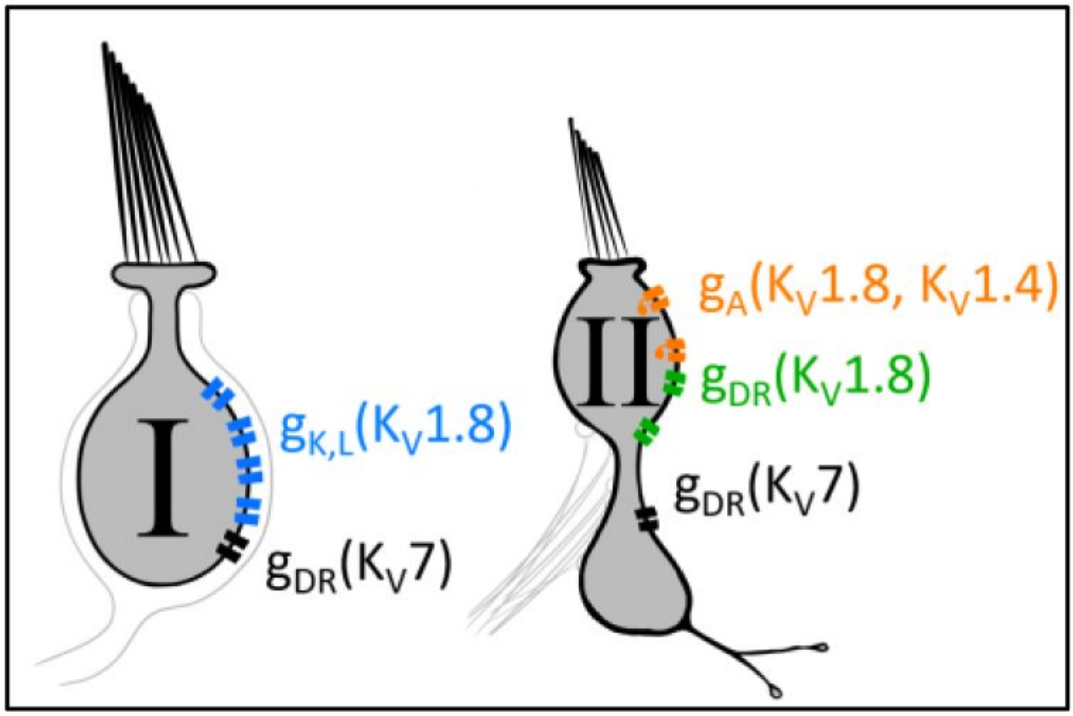

eLife assessment

This study provides direct evidence showing that Kv1.8 channels provide the basis for several potassium currents in the two types of sensory hair cells found in the mouse vestibular system. This is an **important** finding because the nature of the channels underpinning the unusual potassium conductance gK,L in type I hair cells has been under scrutiny for many years. The experimental evidence is **compelling** and the analysis is rigorous. The study will be of interest to cell and molecular biologists, and vestibular and auditory neuroscientists.

https://doi.org/10.7554/eLife.94342.2.sa4

Introduction

The receptor potentials of hair cells (HCs) are strongly shaped by large outwardly rectifying K^+ conductances that are differentially expressed according to HC type. Here we report that a specific voltage-gated K^+ (K_V) channel subunit participates in very different K_V channels dominating the membrane conductances of type I and type II HCs in amniote vestibular organs.

Type I HCs occur only in amniote vestibular organs. Their most distinctive features are that they are enveloped by a calyceal afferent terminal (Wersäll, 1956; Lysakowski and Goldberg, 2004) and that they express $g_{K,L}$ (Correia and Lang, 1990; Rennie and Correia, 1994; Rüsch and Eatock, 1996a): a large non- inactivating conductance with an activation range from –100 to –60 mV, far more negative than other "low-voltage-activated" K_V channels. HCs are known for their

large outwardly rectifying K+ conductances, which repolarize membrane voltage following a mechanically evoked perturbation and in some cases contribute to sharp electrical tuning of the hair cell membrane. $g_{K,L}$ is unusually large and unusually negatively activated, and therefore strongly attenuates and speeds up the receptor potentials of type I HCs (Correia et al., 1996; Rüsch and Eatock, 1996b). In addition, $g_{K,L}$ augments non-quantal transmission from type I HC to afferent calyx by providing open channels for K^+ flow into the synaptic cleft (Contini et al., 2012, 2017, 2020; Govindaraju et al., 2023), increasing the speed and linearity of the transmitted signal (Songer and Eatock, 2013).

Type II HCs have compact afferent synaptic contacts (boutons) where the receptor potential drives quantal release of glutamate. They have fast-inactivating (A-type, g_A) and delayed rectifier (g_{DR}) conductances that are opened by depolarization above resting potential (V_{rest}).

The unusual properties of $g_{K,L}$ have long attracted curiosity about its molecular nature. $g_{K,L}$ has been proposed to include "M-like" K_V channels in the K_V7 and/or erg channel families (Kharkovets et al., 2000; Hurley et al., 2006; Holt et al., 2007). The $K_V7.4$ subunit was of particular interest because it contributes to the low-voltage-activated conductance, $g_{K,n}$, in cochlear outer hair cells, but was eventually eliminated as a $g_{K,L}$ subunit by experiments on $K_V7.4$-null mice (Spitzmaul et al., 2013).

Several observations suggested the $K_V1.8$ (KCNA10) subunit as an alternative candidate for $g_{K,L}$. $K_V1.8$ is highly expressed in vestibular sensory epithelia (Carlisle et al., 2012), particularly hair cells (Lee et al., 2013; Scheffer et al., 2015; McInturff et al., 2018), with slight expression elsewhere (skeletal muscle, Lee et al., 2013; kidney, Yao, 2002). $K_V1.8^{-/-}$ mice show absent or delayed vestibular-evoked potentials, the synchronized activity of afferent nerve fibers sensitive to fast linear head motions (Lee et al., 2013). Unique among K_V1 channels, $K_V1.8$ has a cyclic nucleotide binding domain (Lang et al., 2000) with the potential to explain $g_{K,L}$'s known cGMP dependence (Behrend et al., 1997; Chen and Eatock, 2000).

Our comparison of whole-cell currents and immunohistochemistry in type I HCs from $K_V1.8^{-/-}$ and $K_V1.8^{+/+,+/-}$ mouse utricles confirmed that $K_V1.8$ expression is necessary for $g_{K,L}$. More surprisingly, $K_V1.8$ expression is also required for A-type and delayed rectifier conductances of type II HCs. In both HC types, eliminating the $K_V1.8$-dependent major conductances revealed a smaller delayed rectifier conductance involving K_V7 channels. Thus, the distinctive outward rectifiers that produce such different receptor potentials in type I and II HCs both include $K_V1.8$ and K_V7 channels.

Results

We compared whole-cell voltage-activated K^+ currents in type I and type II hair cells from homozygous knockout ($K_V1.8^{-/-}$) animals and their wildtype ($K_V1.8^{+/+}$) or heterozygote ($K_V1.8^{+/-}$) littermates. We immunolocalized $K_V1.8$ subunits in the utricular epithelium and pharmacologically characterized the residual K^+ currents of $K_V1.8^{-/-}$ animals. Current clamp experiments demonstrated the impact of $K_V1.8$- dependent currents on passive membrane properties.

We recorded from three utricular zones: lateral extrastriola (LES), striola, and medial extrastriola (MES) (**Fig. 3A.1**); striolar and extrastriolar zones have many structural and functional differences and give rise to afferents with different physiology (reviewed in Goldberg, 2000; Eatock and Songer, 2011). Recordings are from 412 type I and II HCs (53% LES, 30% MES, 17% striola) from mice between postnatal day (P) 5 and P370. We recorded from such a wide age range

to test for developmental or senescent changes in the impact of the null mutation. Above P18, we did not see substantial changes in K_V channel properties, as reported (González-Garrido et al., 2021).

$K_V1.8^{-/-}$ animals appeared to be healthy and to develop and age normally, as reported (Lee et al., 2013), and hair cells were healthy (see Methods for criteria).

KV1.8 is necessary for gK,L in type I hair cells

The large low-voltage activated conductance, $g_{K,L}$, in $K_V1.8^{+/+,+/-}$ type I hair cells produces distinctive whole- cell current responses to voltage steps, as highlighted by our standard type I voltage protocol (**Fig. 1A**). From a holding potential within the $g_{K,L}$ activation range (here –74 mV), the cell is hyperpolarized to –124 mV, negative to E_K and the activation range, producing a large inward current through open $g_{K,L}$ channels that rapidly decays as the channels deactivate. We use the large transient inward current as a hallmark of $g_{K,L}$. The hyperpolarization closes all channels, and then the activation function is probed with a series of depolarizing steps, obtaining the maximum conductance from the peak tail current at –44 mV (**Fig. 1A**). We detected no difference between the Boltzmann parameters of $g_{K,L}$ G-V curves from $K_V1.8^{+/-}$ and $K_V1.8^{+/+}$ type I HCs.

For a similar voltage protocol, $K_V1.8^{-/-}$ type I HCs (**Fig. 1B**) produced no inward transient current at the step from –74 mV to –124 mV and much smaller depolarization-activated currents during the iterated steps, even at much more positive potentials. **Figure 1C** compares the conductance-voltage (G-V, activation) curves fit to tail currents (**Eq. 1**; see insets in **Fig. 1A-B**): the maximal conductance (g_{max}) of the $K_V1.8^{-/-}$ HC was over 10-fold smaller (**Fig. 1C.1**), and the curve was positively shifted by >40 mV (**Fig. 1C.2**). **Figure 1D** shows the G-V Boltzmann fit parameters for type I HCs from mice >P12, an age at which type I HCs normally express $g_{K,L}$ (Rüsch et al., 1998).

Suppl. Fig. 1 shows how G-V parameters of outwardly rectifying currents in type I HCs changed from P5 to P360. In $K_V1.8^{+/+,+,-}$ mice, the parameters transitioned over the first 15-20 postnatal days from values for a conventional delayed rectifier, activating positive to resting potential, to $g_{K,L}$ values, as previously described (Rüsch et al., 1998; Géléoc et al., 2004; Hurley et al., 2006). Between P5 and P10, some type I HCs have not yet acquired the physiologically defined conductance, $g_{K,L}$. No effects of $K_V1.8$ deletion were seen in the delayed rectifier currents of immature type I HCs (**Suppl. Fig. 1B**), showing that they were not immature forms of the $K_V1.8$-dependent $g_{K,L}$ channels.

$K_V1.8^{-/-}$ type I HCs had a much smaller residual delayed rectifier that activated positive to resting potential, with V_{half} ~–40 mV and g_{max} density of 1.3 nS/pF. No additional K^+ conductance activated up to +40 mV, and G-V parameters did not change much with age from P5 to P370. We characterize this $K_V1.8$- independent delayed rectifier later. A much larger non-$g_{K,L}$ delayed rectifier conductance ("$g_{DR,I}$") was reported in our earlier publication on mouse utricular type I HCs (Rüsch et al., 1998). This current was identified as that remaining after "blocking" $g_{K,L}$ with 20 mM external Ba^{2+}. Our new data suggest that there is no large non-$g_{K,L}$ conductance, and that instead high Ba^{2+} positively shifted the apparent voltage dependence of $g_{K,L}$.

KV1.8 strongly affects type I passive properties and responses to current steps

While the cells of $K_V1.8^{-/-}$ and $K_V1.8^{+/-}$ epithelia appeared healthy, type I hair cells had smaller membrane capacitances (C_m): 4-5 pF in $K_V1.8^{-/-}$ type I HCs, ~20% smaller than $K_V1.8^{+/-}$ type I HCs (~6 pF) and ~30% smaller than $K_V1.8^{+/+}$ type I HCs (6-7 pF; **Table 2**). C_m scales with surface area, but soma sizes were unchanged by deletion of $K_V1.8$ (**Suppl. Table 2**). Instead, C_m may be higher in $K_V1.8^{+/+}$ cells because of $g_{K,L}$ for two reasons. First, highly expressed trans-membrane

Figure 1.

KV1.8$^{-/-}$ type I hair cells lacked gK,L, the dominant conductance in mature KV1.8$^{+/+,+/-}$ type I HCs.

Representative voltage-evoked currents in **(A)** a P22 KV1.8$^{+/-}$ type I HC and **(B)** a P29 KV1.8$^{-/-}$ type I HC. (A) *Arrow,* transient inward current that is a hallmark of gK,L. *Arrowheads,* tail currents, magnified in *insets*. For steps positive to the midpoint voltage, tail currents are very large. As a result, K^+ accumulation in the calyceal cleft reduces driving force on K^+, causing currents to decay rapidly, as seen in A (Lim et al., 2011). Note that the voltage protocol (top) in B extends to more positive voltages. **(C)** Activation (G-V) curves from tail currents in A and B; symbols, data; curves, Boltzmann fits (Eq. 1). **(D)** Fit parameters from mice >P12 show big effect of KV1.8$^{-/-}$ and no difference between KV1.8$^{+/-}$ and KV1.8$^{+/+}$. *Asterisks* (here and elsewhere): *, p<0.05; **, p<0.01; ***, p<0.001; and ****, p<0.0001. *Line,* median; *Box,* interquartile range; *Whiskers*, outliers. See **Table 1** for statistics.

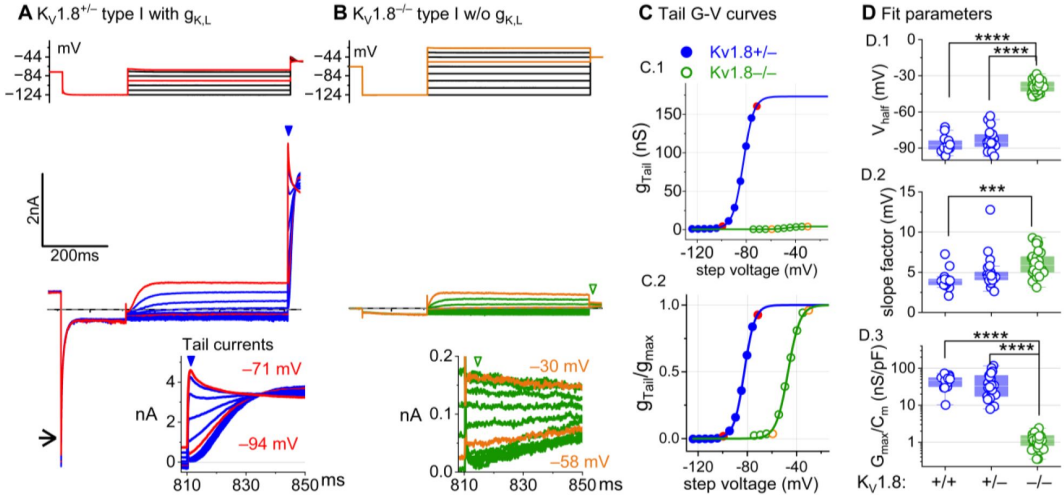

Table 1.

Type I hair cell K_V activation voltage dependence and kinetics. Mean ± SEM (number of cells). g is effect size, Hedge's g. KWA is Kruskal-Wallis ANOVA.

Zone	K_V1.8	Tail $V_{1/2}$, mV [a]	Tail S, mV [b]	Tail G_{max}, nS [c]	Tail G_{max}/C_m, nS/pF [d]	Age (median, range)
Extrastriola	+/+	−85 ± 2 (12)	4.3 ± 0.4 (12)	270 ± 40 (11)	47 ± 8 (11)	22, 14-287
	+/–	−83 ± 1 (40)	5.2 ± 0.3 (40)	210 ± 20 (40)	37 ± 4 (40)	19, 13-259
	–/–	−40.2 ± 0.9 (26)	5.7 ± 0.3 (26)	5.4 ± 0.3 (26)	1.11 ± 0.08 (26)	45, 14-277
Striola	+/+	−87 ± 3 (6)	4.3 ± 0.3 (6)	310 ± 70 (6)	41 ± 7 (6)	40, 15-59
	+/–	−88 ± 2 (3)	4.7 ± 0.9 (3)	270 ± 60 (3)	44 ± 6 (3)	19, 14-20
	–/–	−38 ± 1 (13)	6.2 ± 0.4 (13)	6.5 ± 0.6 (13)	1.5 ± 0.1 (13)	202, 14-370

[a] –/– vs +/+: 2-way ANOVA, p < 1E-9, g 7.7; –/– vs +/–: 2-way ANOVA, p < 1E-9, g 6.8
[b] –/– vs +/+: 2-way ANOVA, p = 8.4E-4, g 1.2
[c] –/– vs +/+: 2-way ANOVA, p < 1E-9, g 3.7; –/– vs +/–: 2-way ANOVA, p < 1E-9, g 2.1
[d] –/– vs +/+: 2-way ANOVA, p < 1E-9, g 3.6; –/– vs +/–: 2-way ANOVA, p < 1E-9, g 2.0

proteins (see discussion of $g_{K,L}$ channel density in Chen and Eatock, 2000) can affect membrane thickness (Mitra et al., 2004), which is inversely proportional to specific C_m. Second, $g_{K,L}$ could contaminate estimations of capacitive current, which is calculated from the decay time constant of transient current evoked by a small voltage step *outside* the operating range of any ion channels. $g_{K,L}$ has such a negative operating range that, even for V_m negative to –90 mV, some $g_{K,L}$ channels are voltage-sensitive and could add to capacitive current.

Basolateral conductances help set the resting potential and passive membrane properties that regulate the time course and gain of voltage responses to small currents. To examine the effect of $K_V1.8$ on these properties, we switched to current clamp mode and measured resting potential (V_{rest}), input resistance (R_{in}, equivalent to voltage gain for small current steps, △V/△I), and membrane time constant (τ_{RC}). In $K_V1.8^{-/-}$ type I HCs, V_{rest} was much less negative (**Fig. 2A.1**), R_{in} was greater by ~20-fold (**Fig. 2A.2**), and membrane charging times were commensurately longer (**Fig. 2A.3**).

The differences between the voltage responses of $K_V1.8^{+/+,+/-}$ and $K_V1.8^{-/-}$ type I HCs are expected from the known impact of $g_{K,L}$ on V_{rest} and R_{in} (Correia and Lang, 1990; Ricci et al., 1996; Rüsch and Eatock, 1996b; Songer and Eatock, 2013). The large K^+-selective conductance at V_{rest} holds V_{rest} close to E_K (K^+ equilibrium potential) and minimizes gain (△V/△I), such that voltage-gated conductances are negligibly affected by the input current and the cell produces approximately linear, static responses to iterated current steps. For $K_V1.8^{-/-}$ type I HCs, with their less negative V_{rest} and larger R_{in}, positive current steps evoked a fast initial depolarization (**Fig. 2B.2**), activating residual delayed rectifiers and repolarizing the membrane toward E_K. Negative current steps evoked an initial "sag" (**Fig. 2B.2**), a hyperpolarization followed by slow repolarization as the HCN1 channels open (Rüsch and Eatock, 1996b; Horwitz et al., 2011).

Overall, comparison of the $K_V1.8^{+/+,+/-}$ and $K_V1.8^{-/-}$ responses shows that with $K_V1.8$ ($g_{K,L}$), the voltage response of the type I hair cell is smaller but better reproduces the time course of the input current.

KV1.8 is necessary for both inactivating and non-inactivating KV currents in type II hair cells

Type II HCs also express $K_V1.8$ mRNA (McInturff et al., 2018; Orvis et al., 2021). Although their outwardly- rectifying conductances (g_A and g_{DR}) differ substantially in voltage dependence and size from $g_{K,L}$, both conductances were strongly affected by the null mutation: g_A was eliminated and the delayed rectifier

was substantially smaller. Below we describe g_A and g_{DR} in $K_V1.8^{+/+,+/-}$ type II HCs and the residual outward rectifying current in $K_V1.8^{-/-}$ type II HCs.

$K_V1.8^{+/+,+/-}$ type II HCs

Most (81/84) $K_V1.8^{+/+,+/-}$ type II HCs expressed a rapidly-activating, rapidly- inactivating A-type conductance (g_A). We define A current as the outwardly rectifying current that inactivates by over 30% within 200 ms. g_A was more prominent in extrastriolar zones, as reported (Holt et al. 1999, Weng and Correia 1999).

We compared the activation and inactivation time course and inactivation prominence for 200-ms steps from –124 mV to ~30 mV. Outward currents fit with Eq. 3 yielded fast inactivation time constants ($\tau_{Inact,\ Fast}$) of ~30 ms in LES (**Fig. 3A.2**). $\tau_{Inact,\ Fast}$ was faster in LES than in MES or striola (**Fig. 3A.3**) and fast inactivation was a larger fraction of the total inactivation in LES than striola (~0.5 vs. 0.3, **Fig. 3A.4**).

Table 2.

Type I hair cell passive membrane properties. Mean ± SEM (number of cells). g is effect size, Hedge's g. KWA is Kruskal-Wallis ANOVA.

Zone	$K_V1.8$	V_{rest}, mV [a, b]	R_{input}, MΩ [c]	τ_{RC}, ms [d]	C_m (pF) [e]	Age (median, range)
Extrastriola	+/+	–84 ± 3 (6)	44 ± 6 (6)	0.24 ± 0.03 (6)	6.1 ± 0.4 (13)	19.5, 14-287
	+/–	–88.0 ± 0.7 (28)	55 ± 5 (24)	0.32 ± 0.03 (23)	5.8 ± 0.2 (44)	21, 16-29
	–/–	–63 ± 2 (15)	1400 ± 100 (15)	6.4 ± 0.6 (15)	5 ± 0.2 (27)	45, 14-202
Striola	+/+	–87 ± 2 (4)	50 ± 8 (4)	0.30 ± 0.04 (4)	7.4 ± 0.7 (7)	43, 40-59
	+/–	–87 ± 3 (3)	38 ± 8 (2)	0.21 ± 0.01 (2)	5.9 ± 0.6 (3)	19, 19-20
	–/–	–74 ± 5 (5)	1000 ± 300 (4)	4.2 ± 1.0 (4)	4.4 ± 0.2 (14)	202, 24-370

[a] striolar –/– vs ES –/–: 2-way ANOVA, p = 0.006, g 1.2; striolar –/– vs striolar +/+,+/–: 2-way ANOVA, p = 0.005, g 1.7
[b] –/– vs +/+: 2-way ANOVA, p < 1E-9, g 2.3; –/– vs +/–: 2-way ANOVA, p < 1E-9, g 3.4
[c] –/– vs +/+: 2-way ANOVA, p < 1E-9, g 3.1; –/– vs +/–: 2-way ANOVA, p < 1E-9, g 3.9
[d] –/– vs +/+: 2-way ANOVA, p < 1E-9, g 2.7; –/– vs +/–: 2-way ANOVA, p < 1E-9, g 3.4
[e] –/– vs +/+: 2-way ANOVA, p = 3E-7, g 1.5; –/– vs +/–: 2-way ANOVA, p = 1.3E-4, g 1.0; +/– vs +/+: 2-way ANOVA, p = 0.048, g 0.6

Table 3.

Type II hair cell KV currents: Activation and inactivation time course at +30 mV. Mean ± SEM. g is effect size, Hedge's g. KWA is Kruskal-Wallis ANOVA.

Zone	$K_V1.8$	τ_{Act} at 30 mV, ms [a, b]	$\tau_{Inact,Fast}$ at 30 mV, ms [c, d]	Fast inactivation prominence [e]	Inactivation % [f, g]	N cells	Age (median, range)
LES	+/+	2.11 ± 0.09	23 ± 3	0.46 ± 0.03	45 ± 2	30	46, 14-312
	+/–	1.64 ± 0.09	15 ± 2	0.53 ± 0.03	51 ± 2	27	29, 13-280
	–/–	4.4 ± 0.5	*NA*	*NA*	25 ± 3	21	128, 15-355
MES	+/+	2.8 ± 0.5	50 ± 10	0.40 ± 0.04	42 ± 3	9	94, 22-296
	+/–	2.2 ± 0.2	90 ± 60	0.42 ± 0.03	47 ± 2	15	24, 13-52
	–/–	10 ± 7	*NA*	*NA*	29 ± 5	10	84, 28-355
Striola	+/+	2.7 ± 0.3	50 ± 10	0.31 ± 0.07	39 ± 3	5	45, 40-287
	+/–	2.9 ± 0.4	300 ± 200	0.3 ± 0.06	28 ± 2	5	19, 14-30
	–/–	7 ± 2	*NA*	*NA*	22 ± 2	6	202, 29-298

[a] –/– vs +/+: KWA, p = 0.0048, g 0.6; –/– vs +/–: KWA, p = 2.3E-7, g 0.6
[b] Striola vs LES: KWA, p = 5.7E-4, g 1.0
[c] +/– vs +/+: KWA, p = 0.027, g 0.2
[d] LES vs MES: KWA, p = 0.0018, g 0.3; LES vs Striola: KWA, p = 1.9E-4, g 0.8
[e] LES vs Striola: 2-way ANOVA, p = 0.0041, g 0.7
[f] –/– vs +/+: 2-way ANOVA, p < 1E-9, g 1.7; –/– vs +/–: 2-way ANOVA, p < 1E-9, g 1.8
[g] Striola vs LES: 2-way ANOVA, p = 3.4E-5, g 0.9; Striola vs MES: 2-way ANOVA, p = 0.0011, g 1.0; Interaction between genotype and Zone: 2-way ANOVA, p = 0.026

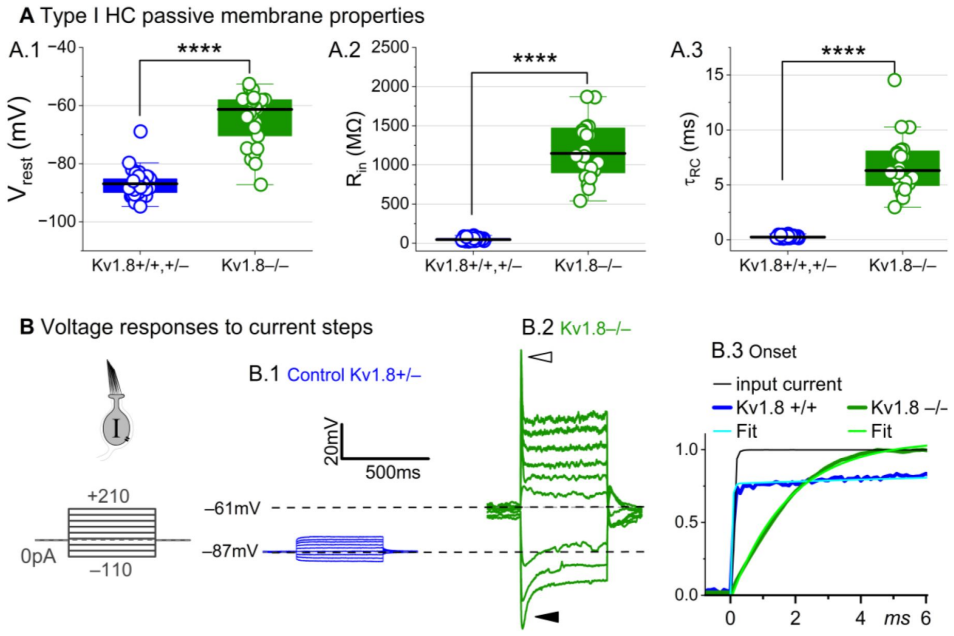

Figure 2.

KV1.8–/– type I hair cells had much longer membrane charging times and higher input resistances (voltage gains) than KV1.8+/+,+/– type I HCs. (A)

gK,L strongly affects passive membrane properties: (**A.1**) Vrest , (**A.2**) Rin, input resistance, and (**A.3**) membrane time constant, τRC = (Rinput * Cm). See **Table 2** for statistics. **(B)** Current clamp responses to the same scale from (B.1) KV1.8+/– and (B.2) KV1.8–/– type I cells, both P29. *Filled arrowhead (B.2),* sag indicating IH activation. *Open arrowhead*, Depolarization rapidly decays as IDR activates. B.3, The 1st 6 ms of voltage responses to 170-pA injection is normalized to steady-state value; overlaid curves are double-exponential fits (KV1.8+/+, τ 40 μs and 2.4 ms) and single-exponential fits (KV1.8–/– , τ 1.1 ms) .

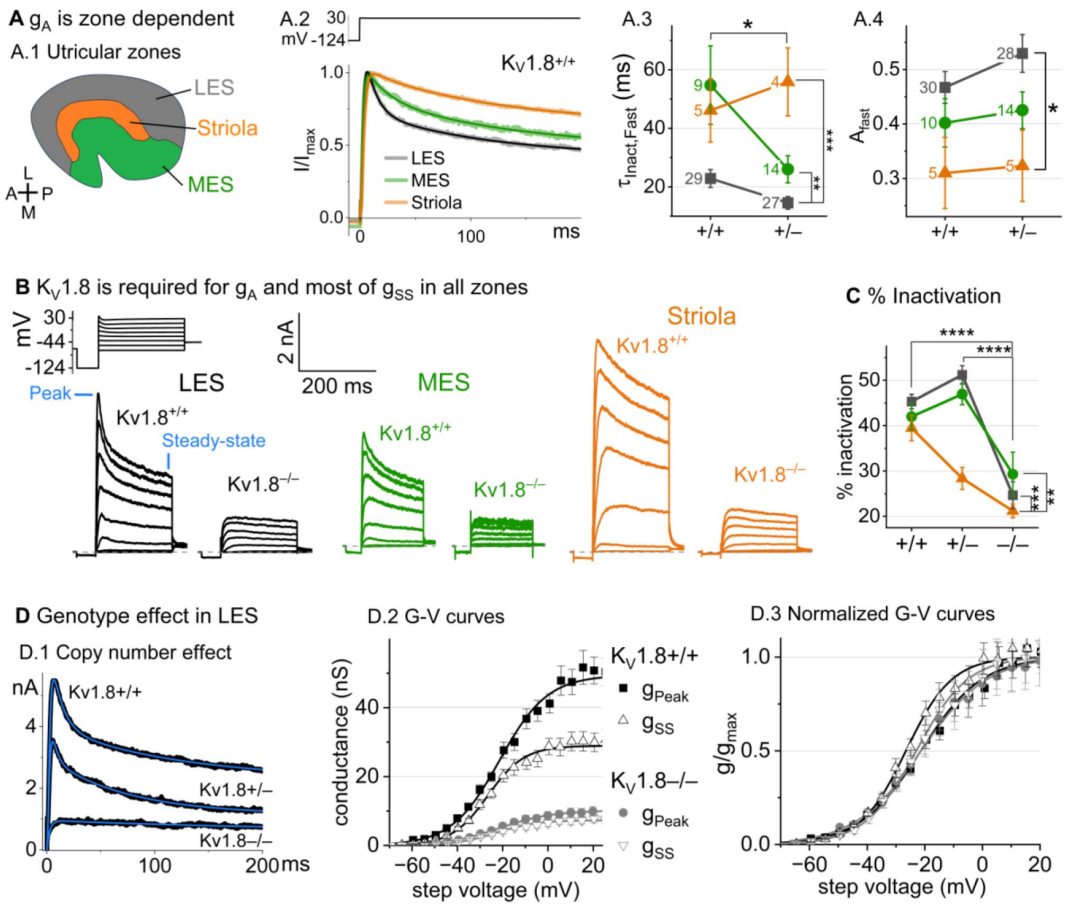

Figure 3.

$K_V1.8^{-/-}$ type II HCs in all zones of the sensory epithelium lacked the major rapidly inactivating conductance, g_A, and had less delayed rectifier conductance. Activation and inactivation varied with epithelial zone and genotype. (**A**) g_A inactivation time course varied across zones. (**A.1**) Zones of the utricular epithelium. (**A.2**) Normalized currents evoked by steps from −124 mV to +30 mV with overlaid fits of **Eq. 3**. (**A.3**) $\tau_{Inact,Fast}$ was faster in $K_V1.8^{+/-}$ than $K_V1.8^{+/+}$ HCs , and faster in LES than other zones. Brackets show post hoc pairwise comparisons between two zones (vertical brackets) and horizontal brackets compare two genotypes; see **Table 3** for statistics. (**A.4**) Fast inactivation was a greater fraction of total inactivation in LES than striola.

(B) Exemplars; ages, *left to right*, P312, P53, P287, P49, P40, P154.

(C) % inactivation at 30 mV was much lower in $K_V1.8^{-/-}$ than $K_V1.8^{+/-}$ and $K_V1.8^{+/+}$, and lower in striola than LES and MES. Interaction between zone and genotype was significant (**Table 3**).

(D) Exemplar currents and G-V curves from LES type II HCs show a copy number effect. (**D.1**) Currents for examples of the 3 genotypes evoked by steps from −124 mV to +30 mV fit with **Eq. 3**. (**D.2**) Averaged peak and steady-state conductance-voltage datapoints from LES cells (+/+, n=37; –/–, n=20) were fit with Boltzmann equations (**Eq. 1**) and normalized by g_{max} in (**D.3**). See **Table 4** for statistics.

To show voltage dependence of activation, we generated G-V curves for peak currents (sum of A-current and delayed rectifier) and steady-state currents measured at 200 ms, after g_A has mostly inactivated (**Figure 3D.2**). $K_V1.8^{+/-}$ HCs had smaller currents than $K_V1.8^{+/+}$ HCs, reflecting a smaller g_{DR} (**Fig. 3D**) and faster fast inactivation (**Fig. 3A.3**). As discussed later, these effects may relate to effects of the $K_V1.8$ gene dosage on the relative numbers of different $K_V1.8$ heteromers.

For $K_V1.8^{+/+}$ and $K_V1.8^{+/-}$ HCs, the voltage dependence as summarized by V_{half} and slope factor (S) was similar. Relative to g_{SS}, g_{Peak} had a more positive V_{half} (~–21 vs. ~–26) and greater S (~12 vs. ~9, **Fig. 3D**, **Table 4**). Because g_{Peak} includes channels with and without fast inactivation, the shallower g_{Peak}-V curve may reflect a more heterogeneous channel population. Only g_{Peak} showed zonal variation, with more positive V_{half} in LES than striola (~–20 mV vs. ~–24 mV, **Fig. 3D**, **Table 4**). We later suggest that variable subunit composition may drive zonal variation in g_{Peak}.

$K_V1.8^{-/-}$ type II HCs

from all zones were missing g_A and 30-50% of g_{DR} (**Fig. 3B-D**). The residual delayed rectifier (1.3 nS/pF) had a more positive V_{half} than g_{DR} in $K_V1.8^{+/+,+/-}$ HCs (~–20 mV *vs.* ~–26 mV, **Fig. 3D.2**). We refer to the $K_V1.8$-dependent delayed rectifier component as $g_{DR}(K_V1.8)$ and to the residual, $K_V1.8$- *in*dependent delayed rectifier component as $g_{DR}(K_V7)$ because, as we show later, it includes K_V7 channels. Supplemental Figure 3A shows the development of $K_V1.8$-dependent and independent K_V currents in type II HCs with age from P5 to over P300. In $K_V1.8^{+/+,+/-}$ type II HCs, g_A was present at all ages with a higher % inactivation after P18 than at P5-P10 (**Suppl. Fig. 3A**.4). g_{Peak} did not change much above P12 except for a compression of conductance density from P13 to P370 (partial correlation coefficient = –0.4, p = 2E-5, **Suppl. Fig. 3A.3**).

We saw small rapidly inactivating outward currents in a minority of $K_V1.8^{-/-}$ type II HCs (23%, 7/30), all >P12 and extrastriolar (**Suppl. Fig. 4**). These currents overlapped with g_A in percent inactivation, inactivation kinetics, and activation voltage dependence but were very small. As discussed later, we suspect that these currents flow through homomers of inactivating K_V subunits that in control hair cells join with $K_V1.8$ subunits and confer inactivation on the heteromeric conductance.

KV1.8 affects type II passive properties and responses to current steps

In type II HCs, absence of $K_V1.8$ did not change V_{rest} (**Fig. 4A.1**) because g_A and g_{DR} both activate positive to rest, but significantly increased R_{in} and τ_{RC} (**Fig. 4A.2-A.3**).

Positive current steps evoked an initial depolarizing transient in both $K_V1.8^{+/+}$ and $K_V1.8^{-/-}$ type II HCs, but the detailed time course differed (**Fig. 4B**). Both transient and steady-state responses were larger in

$K_V1.8^{-/-}$, consistent with their larger R_{in} values

Absence of $K_V1.8$ increased the incidence of sharp electrical resonance in type II HCs. Electrical resonance, which manifests as ringing responses to current steps, can support receptor potential tuning (Ashmore, 1983; Fettiplace, 1987; Hudspeth and Lewis, 1988; Ramanathan and Fuchs, 2002). Larger R_{in} values made $K_V1.8^{-/-}$ type II HCs more prone to electrical resonance; **Figure 4C.1** shows a striking example.

Median resonance quality (Q_e, sharpness of tuning) was greater in $K_V1.8^{-/-}$ (1.33, n=26) than $K_V1.8^{+/+}$ (0.66, n=23) or $K_V1.8^{+/-}$ (0.59, n=44) type II HCs.

Zone	$K_V1.8$	*Peak $V_{1/2}$, mV* [a]	Peak S, mV [b, c]	A-type g_{max}/C_m, nS/pF [d]	SS V_{half}, mV [e]	SS S, mV [f]	SS g_{max}/C_m, nS/pF [g, h]	N cells	Age (median, range)
LES	+/+	–19.8 ± 0.6	11.8 ± 0.4	4.0 ± 0.3	–25.0 ± 0.5	8.7 ± 0.3	7.1 ± 0.8	37	46, 14-312
	+/–	–19.8 ± 0.8	12.8 ± 0.4	3.8 ± 0.3	–26.8 ± 0.8	8.7 ± 0.3	4.9 ± 0.4	35	29, 13-280
	–/–	–18 ± 1	11.7 ± 0.4	0.37 ± 0.05	–19 ± 1	12.1 ± 0.5	1.8 ± 0.2	20	128, 15-355
MES	+/+	–22 ± 1	11 ± 0.7	4.1 ± 0.7	–26 ± 1	8.3 ± 0.5	9 ± 1	11	94, 22-296
	+/–	–21 ± 1	11.8 ± 0.4	3.6 ± 0.5	–27 ± 1	9.0 ± 0.3	5.9 ± 0.7	16	24, 13-52
	–/–	–19 ± 1	10.8 ± 0.6	0.6 ± 0.1	–20 ± 1	10.7 ± 0.7	2.5 ± 0.3	15	84, 28-355
Striola	+/+	–24 ± 1	9.6 ± 0.5	5 ± 1	–26.6 ± 0.9	8.2 ± 0.4	12 ± 1	7	45, 40-287
	+/–	–25 ± 2	9.4 ± 0.4	2.6 ± 0.6	–28 ± 2	8.2 ± 0.3	10 ± 2	6	19, 14-30
	–/–	–21.3 ± 0.9	10.3 ± 0.5	0.7 ± 0.1	–21.7 ± 0.8	10.5 ± 0.6	3.9 ± 0.5	8	202, 29-298

[a] Striola vs LES: 2-way ANOVA, p = 0.00116, g 0.9

[b] Striola vs MES: 2-way ANOVA, p = 0.016, g 0.8; Striola vs LES: 2-way ANOVA, p = 7.5E-6, g 1.2

[c] –/– vs +/–: 2-way ANOVA, p = 0.036, g 0.5

[d] –/– vs +/+: Welch ANOVA, p < 1E-9, g 2.3; –/– vs +/–: Welch ANOVA, p < 1E-9, g 2.3

[e] –/– vs +/+: 2-way ANOVA, p < 1E-9, g 1.4; –/– vs +/–: 2-way ANOVA, p < 1E-9, g 1.6

[f] –/– vs +/+: 2-way ANOVA, p < 1E-9, g 1.4; –/– vs +/–: 2-way ANOVA, p = 4.5E-7, g 1.1

[g] –/– vs +/+: Welch ANOVA, p < 1E-9, g 1.6; –/– vs +/–: Welch ANOVA, p < 1E-9, g 1.3; +/+ vs +/–: Welch ANOVA, p = 0.007, g 1.6

[h] Striola vs LES: 1-way ANOVA, p = 0.001, g 0.9); Striola vs MES: 1-way ANOVA, p = 0.01, g 0.8

Table 4.

Type II hair cell KV currents: Activation voltage dependence. Mean ± SEM. g is effect size, Hedge's g. KWA is Kruskal-Wallis ANOVA.

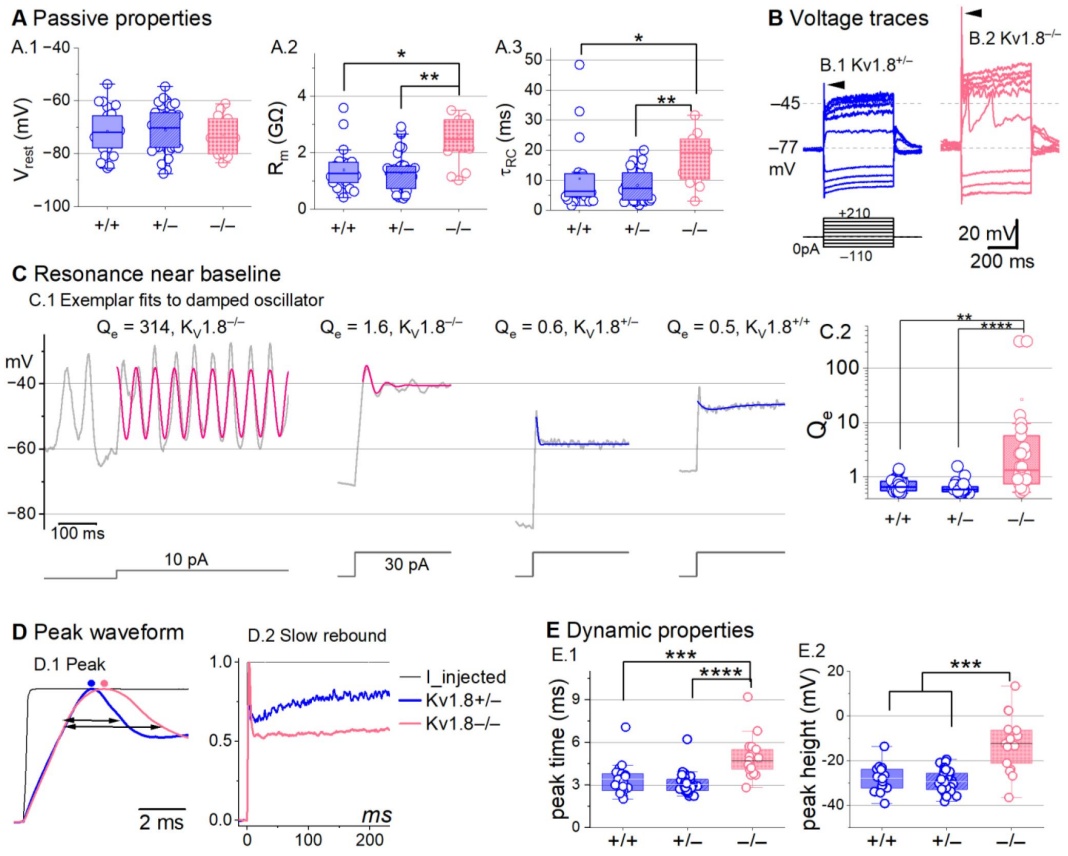

Figure 4.

KV1.8$^{-/-}$ type II hair cells had larger, slower voltage responses and more electrical resonance.

(A) Passive membrane properties near resting membrane potential: A.1) Resting potential. Rinput (A.2) and τRC (A.3) were obtained from single exponential fits to voltage responses < 15 mV. See **Table 5** for statistics.
(**B**) Exemplar voltage responses to iterated current steps (*bottom)* illustrate key changes in gain and resonance with KV1.8 knockout. (**B.1**) KV1.8$^{+/-}$ type II HC (P24, LES) and (**B.2**) KV1.8$^{-/-}$ type II HC (P53, LES). *Arrowheads,* depolarizing transients.
(**C**) Range of resonance illustrated for KV1.8$^{-/-}$ type II HCs (*left, pink curves fit to* ***Eq. 5***) and controls (*right, blue fits*). (**C.1**) *Resonant frequencies, left to right:* 19.6, 18.4, 34.4, 0.3 Hz. Leftmost cell resonated spontaneously (before step). (**C.2**) Tuning quality (Qe; **Eq. 6**) was higher for KV1.8$^{-/-}$ type II HCs (KWA, p = 0.0064 vs. KV1.8$^{+/+}$; p = 7E-8 vs. KV1.8$^{+/-}$).
(**D**) KV1.8$^{-/-}$ type II HCs had higher, slower peaks and much slower rebound potentials in response to large (170-pA) current steps. (**D.1**) Normalized to show initial depolarizing transient (*filled circles*, times of peaks; *horizontal arrows*, peak width at half-maximum). (**D.2**) Longer time scale to highlight how null mutation reduced post-transient rebound.
(**E**) In KV1.8$^{-/-}$ HCs, depolarizing transients evoked by a +90-pA step were slower to peak (**E.1**) and (**E.2**) larger.

Table 5.

Type II hair cell passive membrane properties. Mean ± SEM (number of cells). g is effect size, Hedge's g. KWA is Kruskal-Wallis ANOVA

Zone	K_V1.8	V_{rest}, mV	R_{input}, GΩ [a]	τ_{RC}, ms [b]	Peak height, mV, 170 [c]	Peak time, ms [d]	C_m, pF	Age (median, range)
Extrastriola	+/+	–71 ± 2 (19)	1.4 ± 0.2 (16)	11 ± 3 (16)	–20 ± 2 (15)	2.5 ± 0.2 (15)	4.7 ± 0.2 (50)	45, 16-312
	+/–	–71 ± 2 (34)	1.2 ± 0.1 (27)	9 ± 1 (27)	–20 ± 1 (30)	2.44 ± 0.08 (30)	4.6 ± 0.1 (52)	27, 13-280
	–/–	–76 ± 2 (9)	2.3 ± 0.3 (7)	16 ± 3 (7)	2 ± 6 (7)	3.6 ± 0.3 (7)	4.6 ± 0.2 (35)	53, 15-154
Striola	+/+	–73.1 ± 1.0 (6)	1.4 ± 0.1 (6)	9 ± 1 (6)	–20 ± 2 (5)	2.7 ± 0.1 (5)	4.6 ± 0.2 (7)	45, 40-224
	+/–	–71 ± 3 (5)	1.4 ± 0.3 (6)	7 ± 2 (6)	–20 ± 2 (6)	2.3 ± 0.1 (6)	4.8 ± 0.2 (6)	19, 19-30
	–/–	–68 ± 2 (6)	3.0 ± 0.7 (6)	26 ± 10 (6)	2 ± 7 (4)	4 ± 1 (4)	4.4 ± 0.3 (7)	178, 29-298

[a] –/– vs +/+: KWA, p = 0.015, g 1.2; –/– vs +/–: KWA, p = 0.002, g 1.5
[b] –/– vs +/+: KWA, p = 0.016, g 0.7; –/– vs +/–: KWA, p = 0.008, g 1.2
[c] –/– vs +/+: KWA, p = 0.006, g 2.1; –/– vs +/–: KWA, p = 2E-4, g 2.6
[d] –/– vs +/+: 2-way ANOVA, p <1E-9, g 1.3; –/– vs +/–: 2-way ANOVA, p < 1E-9, g 1.9

Table 6.

Key Resources Table

Antibody	Source	Catalog Number	Lot Number	Dilution
Rabbit anti-K_V1.8	Alomone	APC-157	0102	1:200 or 1:400
Mouse anti-K_V1.4	NeuroMab	P15385	5HK-05	1:400
Mouse IGg2a-conjugated anti-Tuj1	Covance	MMS-435P	B205808	1:300
Goat anti-calretinin	Millipore	AB1550	9669	1:600
Mouse IgG1-conjugated anti-K_V7.4	NeuroMab	2HK-65		1:200
Donkey anti-Rabbit Secondary Antibody, Alexa Fluor 594	Invitrogen	A21207	8652	1:200
Donkey anti-Goat 488 nm	Invitrogen	A21125	1920483	1:200
Goat anti-Mouse IgG1 594	Invitrogen	A11055	1869589	1:200
Chemicals and Peptides	Source	Catalog Number	Diluent	
Iberiotoxin	Alomone	STI-400	Water	
XE991 dihydrochloride	Sigma	X2254	Water	
ZD7288	Tocris	APN18035-2	Water	
Bovine serum albumin	Fisher	BP671	water	

$K_V1.8$ affected the time course of the initial peak in response to much larger current injections (**Fig. 4D-E**). Fast activation of g_A in control type II HCs rapidly repolarizes the membrane and then inactivates, allowing the constant input current to progressively depolarize the cell, producing a slow rebound (**Fig 4D.2**). This behavior has the potential to counter mechanotranduction adaptation (Vollrath and Eatock, 2003).

KV1.8 immunolocalized to basolateral membranes of both type I and II HCs

If $K_V1.8$ is a pore-forming subunit in the $K_V1.8$-dependent conductances $g_{K,L}$, g_A, and g_{DR}, it should localize to hair cell membranes. **Figure 5** compares $K_V1.8$ immunoreactivity in $K_V1.8^{+/+}$ and $K_V1.8^{-/-}$ utricles, showing specific immunoreactivity along the basolateral membranes of both hair cell types in $K_V1.8^{+/+}$ utricles. To identify hair cell type and localize the hair cell membrane, we used antibodies against $K_V7.4$ (KCNQ4), an ion channel densely expressed in the calyceal "inner-face" membrane next to the synaptic cleft (Hurley et al., 2006; Lysakowski et al., 2011), producing a cup-like stain around type I HCs (**Fig. 5A**). $K_V1.8$ immunoreactivity was present in hair cell membrane apposing $K_V7.4$-stained calyx inner face in $K_V1.8^{+/+}$ utricles (**Fig. 5A.1, A.2**) and not in $K_V1.8^{-/-}$ utricles (**Fig. 5A.3**).

In other experiments, we used antibodies against calretinin (Calb2), a cytosolic calcium binding protein expressed by many type II HCs and also by striolar calyx-only afferents (Desai et al., 2005; Lysakowski et al., 2011) (**Fig. 5B**). A hair cell is type II if it is calretinin-positive (**Fig. 5B.1**) or if it lacks a $K_V7.4$-positive or calretinin-positive calyceal cup (**Fig. 5A.2**, **Fig. 5B.3, rightmost cells**). Hair cell identification was confirmed with established morphological indicators: for example, type II HCs tend to have basolateral processes (feet) (Pujol et al., 2014) and, in the extrastriola, more apical nuclei than type I HC.

Previously, Carlisle et al. (2012) reported $K_V1.8$-like immunoreactivity in many cell types in the inner ear. In contrast, Lee et al. (2013) found that gene expression reporters indicated expression only in hair cells and some supporting cells. Here, comparison of control and null tissue showed selective expression of HC membranes, and that some supporting cell staining is non-specific.

KV1.4 may also contribute to gA

Results with the $K_V1.8$ knockout suggest that type II hair cells have an inactivating K_V1 conductance that includes $K_V1.8$ subunits. $K_V1.8$, like most K_V1 subunits, does not show fast inactivation as a heterologously expressed homomer (Lang et al., 2000; Ranjan et al., 2019; Dierich et al., 2020), nor do the $K_V1.8$- dependent channels in type I HCs, as we show, and in cochlear inner hair cells (Dierich et al., 2020). K_V1 subunits without intrinsic inactivation can produce rapidly inactivating currents by associating with $K_V\beta1$ (KCNB1) or $K_V\beta3$ subunits. $K_V\beta1$ is present in type II HCs alongside $K_V\beta2$ (McInturff et al., 2018; Jan et al., 2021; Orvis et al., 2021), which does not confer rapid inactivation (Dwenger et al., 2022).

Another possibility is that in type II HCs, $K_V1.8$ subunits heteromultimerize with $K_V1.4$ subunits—the only K_V1 subunits which, when expressed as a homomer, have complete N-type (fast) inactivation (Stühmer et al., 1989). Multiple observations support this possibility. $K_V1.4$ has been linked to g_A in pigeon type II HCs (Correia et al., 2008) and is the second-most abundant K_V1 transcript in mammalian vestibular HCs, after $K_V1.8$ (Scheffer et al., 2015). $K_V1.4$ is expressed in type II HCs but not type I HCs (McInturff et al., 2018; Orvis et al., 2021), and is not found in striolar HCs (Jan et al., 2021; Orvis et al., 2021), where even in type II HCs, inactivation is slower and less extensive (**Fig. 3A**).

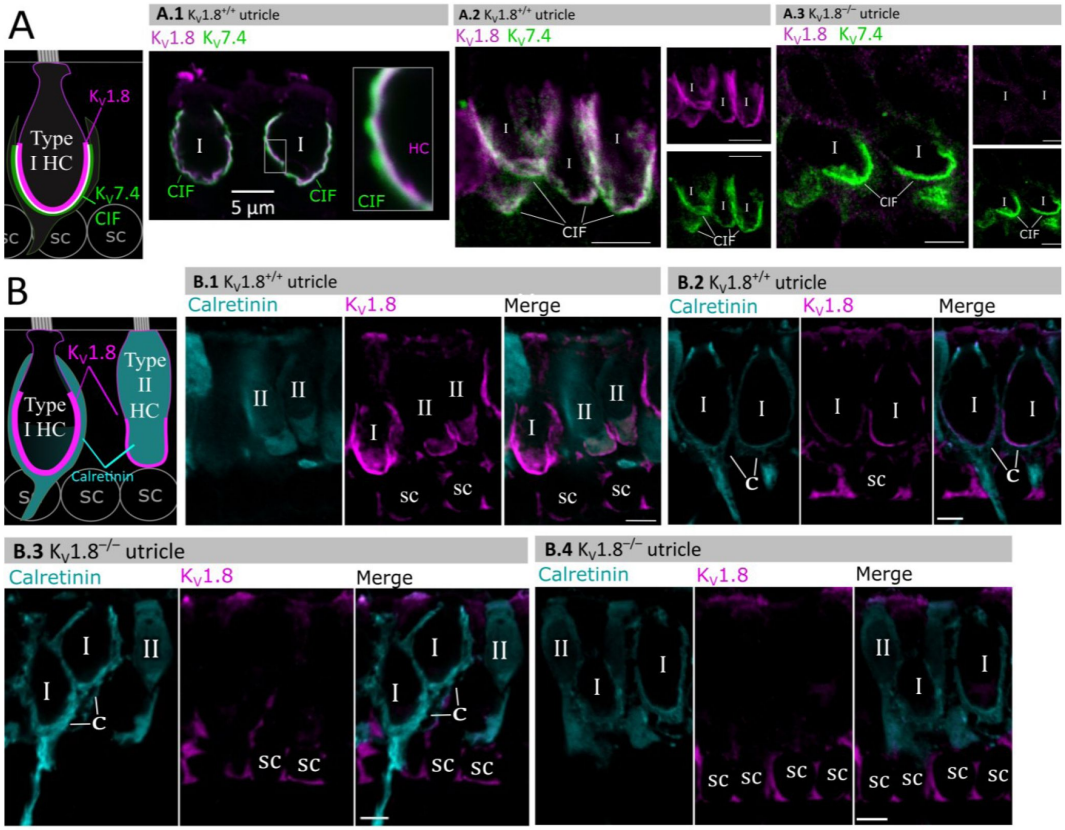

Figure 5.

Type I and type II HC basolateral membranes show specific immunoreactivity to Kv1.8 antibody (magenta).

Antibodies for $K_V7.4$ (A, green) and calretinin (B, cyan) were used as counterstains for calyx membrane (Kv7.4), type II HC cytoplasm (calretinin) and cytoplasm of striolar calyx-only afferents (calretinin). (**A**) *Left,* Cartoon showing $K_V7.4$ on the calyx inner face membrane (CIF) and $K_V1.8$ on the type I HC membrane. SC, supporting cell nuclei. *A.1-3*, Adult mouse utricle sections. $K_V7.4$ antibody labeled calyces on two $K_V1.8$-positive type I HCs (**A.1**), four $K_V1.8$-positive type I HCs (**A.2**), and two $K_V1.8$-negative type I HCs from a $K_V1.8^{-/-}$ mouse (**A.3**).
(**B**) *Left,* Cartoon showing cytoplasmic calretinin stain in calyx-only striolar afferents and most type II HCs, and $K_V1.8$ on membranes of both HC types. In wildtype utricles, $K_V1.8$ immunolocalized to basolateral membranes of type I and II HCs (**B.1**). $K_V1.8$ immunolocalized to type I HCs in striola (**B.2**). Staining of supporting cell (SC) membranes by Kv1.8 antibody was non-specific, as it was present in $K_V1.8^{-/-}$ tissue (**B.3, B.4**).

Functional heteromers form between $K_V1.4$ and other $K_V1.x$ and/or $K_V\beta1$ (Imbrici et al., 2006; Correia et al., 2008; Al-Sabi et al., 2011). Although $K_V1.4$ and $K_V1.8$ heteromers have not been studied directly, g_A's inactivation time course ($\tau_{Fast,Inac}$ of ~30 ms +30 mV, **Fig. 3A**) and voltage dependence (V_{half} –41 mV, **Fig. 6B**) are consistent with these other $K_V1.4$-containing heteromers.

K_V7 channels contribute a small delayed rectifier in type I and type II hair cells

In $K_V1.8^{-/-}$ HCs, absence of $I_{K,L}$ and I_A revealed smaller delayed rectifier K^+ currents that, unlike $I_{K,L}$, activated positive to resting potential and, unlike I_A, lacked fast inactivation. Candidate channels include members of the K_V7 (KCNQ, M-current) family, which have been identified previously in rodent vestibular HCs (Kharkovets et al., 2000; Rennie et al., 2001; Hurley et al., 2006; Scheffer et al., 2015).

We test for K_V7 contributions in $K_V1.8^{-/-}$ type I HCs, $K_V1.8^{-/-}$ type II HCs, and $K_V1.8^{+/+,+/-}$ type II HCs of multiple ages by applying XE991 at 10 μM (**Fig. 7A**), a dose selective for K_V7 channels (Brown et al., 2002) and close to the IC_{50} (Alexander et al., 2019). In $K_V1.8^{-/-}$ HCs of both types, 10 μM XE991 blocked about half of the residual K_V conductance (**Fig. 7B.1**), consistent with K_V7 channels conducting most or all of the non-$K_V1.8$ delayed rectifier current. In all tested HCs (P8-355, median P224), the XE991-sensitive conductance did not inactivate substantially within 200 ms at any voltage, consistent with $K_V7.2$, 7.3, 7.4, and 7.5 currents (Wang, 1998; Kubisch et al., 1999; Schroeder et al., 2000; Jensen et al., 2007; Xu et al., 2007). We refer to this component as $g_{DR}(K_V7)$. The voltage dependence and Gmax density (G_{max}/C_m) of $g_{DR}(K_V7)$ were comparable across HC types and genotypes (**Figure 7B.2-4**). Although $K_V7.4$ was not detectable in HCs during immunostaining (**Fig. 5**), $K_V7.4$ has been shown in type I HCs with immunogold labeling (Kharkovets et al., 2000; Hurley et al., 2006).

These results are consistent with similar K_V7 channels contributing a relatively small delayed rectifier in both HC types. In addition, the similarity of XE991-sensitive currents of $K_V1.8^{+/+}$ and $K_V1.8^{-/-}$ type II HCs indicates that knocking out $K_V1.8$ did not cause general effects on ion channel expression. We did not test XE991 on $K_V1.8^{+/+,+/-}$ type I HCs because $g_{K,L}$ runs down in ruptured patch recordings (Rüsch and Eatock, 1996a; Chen and Eatock, 2000; Hurley et al., 2006), which could contaminate the XE991-sensitive conductance obtained by subtraction.

In one striolar $K_V1.8^{-/-}$ type I HC, XE991 also blocked a small conductance that activated negative to rest (**Suppl. Fig. 5A-B**). This conductance (V_{half} ~= –100 mV, **Suppl. Fig. 5C**) was detected only in $K_V1.8^{-/-}$ type I HCs from the striola (5/23 vs. 0/45 extrastriolar). The V_{half} and $\tau_{deactivation}$ were similar to values reported for $K_V7.4$ channels in cochlear HCs (Wong et al., 2004; Dierich et al., 2020). This very negatively activating K_V7 conductance coexisted with the larger more positively activating K_V7 conductance (**Suppl. Fig. 5C**) and was too small (<0.5 nS/pF) to contribute significantly to $g_{K,L}$ (~10-100 nS/pF, **Fig. 1D**).

Other channels

While our data are consistent with $K_V1.8$- and K_V7- containing channels carrying most of the outward- rectifying current in mouse utricular hair cells, there is evidence in other preparations for additional channels, including K_V11 (KCNH, Erg) channels in rat utricular type I hair cells (Hurley et al., 2006) and BK (KCNMA1) channels in rat utricle and rat and turtle semicircular canal hair cells (Schweizer et al., 2009; Contini et al., 2020).

BK is expressed in mouse utricular hair cells (McInturff et al., 2018; Jan et al., 2021; Orvis et al., 2021). However, Ca^{2+}-dependent currents have not been observed in mouse utricular HCs, and we found little to no effect of the BK-channel blocker iberiotoxin at a dose (100 nM) well beyond the IC_{50}: percent blocked at –30 mV was 2 ± 6% (3 $K_V1.8^{-/-}$ type I HCs); 1 ± 5% (5 $K_V1.8^{+/+,+/-}$ type II

Figure 6.

Inactivation curve of gA in extrastriolar type II HCs.

(**A**) Modified voltage protocol measured accumulated steady-state inactivation in the tail potential. 100 µM ZD7288 in bath prevented contamination by HCN current. (**B**) Voltage dependence of gA's steady-state inactivation (h∞ curve) and peak activation are consistent with KV1.4 heteromers. H∞ curves have overlapped normalized activation (peak conductance, black squares) and inactivation (tail conductance, red circles) G-V data points. *Curves,* Boltzmann fits (**Eq. 1**). *Average fit parameters* from KV1.8$^{+/+,+/-}$ type II HCs, P40-P210, median P94. Inactivation: Vhalf, –42 ±2 mV (n=11); S, 11 ± 1 mV. Activation: Vhalf, –23 ± 1 mV (n=11); S, 11.2 ± 0.4 mV.

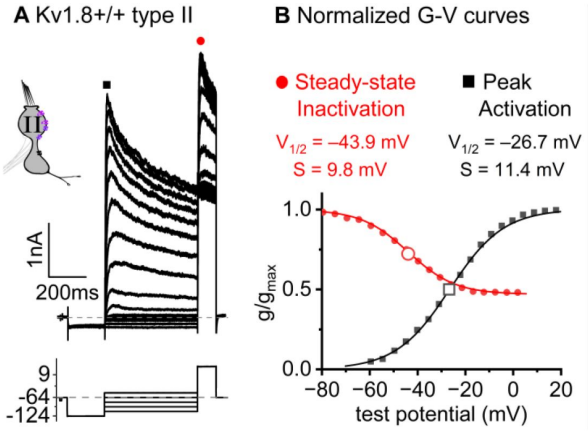

Figure 7.

A KV7-selective blocker, XE991, reduced residual delayed rectifier currents in KV1.8$^{-/-}$ type I and II HCs.

(A) XE991 (10 µM) partly blocked similar delayed rectifier currents in type I and type II KV1.8$^{-/-}$ HCs and a type II KV1.8$^{+/+}$ HC. **(B)** Properties of XE991-sensitive conductance, gDR(KV7). (**B.1**) % Block of steady-state current. (**B.2**) tail G-V curves for KV1.8$^{-/-}$ type I HCs (n=8), KV1.8$^{-/-}$ type II HCs (9), and KV1.8$^{+/+}$ type II HCs (5); mean ± SEM. (**B.3**) Vhalf was less negative in KV1.8$^{+/+}$ type II than KV1.8$^{-/-}$ type I HC (p = 0.01, KWA). (**B.4**) Conductance density was similar in all groups (ANOVA, non-significant at 40% power (*left*), 20% power (*right*).

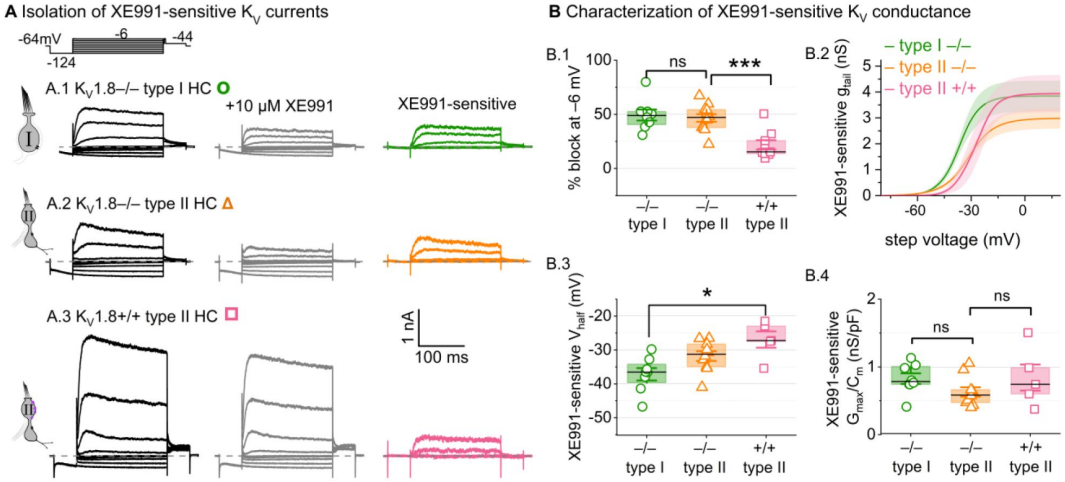

HCs); 7% and 14% (2 $K_V1.8^{-/-}$ type II HCs). We also did not see N-shaped I-V curves typical of many Ca^{2+}-dependent K^+ currents. In our ruptured-patch recordings, Ca^{2+}-dependent BK currents and erg channels may have been eliminated by wash-out of the hair cells' small Ca_V currents (Bao et al., 2003) or cytoplasmic second messengers (Hurley et al., 2006).

To check whether the constitutive $K_V1.8$ knockout has strong non-specific effects on channel trafficking, we examined the summed HCN and fast inward rectifier currents (I_H and I_{Kir}) at –124 mV, and found them similar across genotypes (**Suppl. Fig. 6**). The $g_{K,L}$ knockout allowed identification of zonal differences in I_H and I_{Kir} in type I HCs, previously examined in type II HCs (Masetto and Correia, 1997; Levin and Holt, 2012). In type I HCs from both control and null utricles, I_H and I_{Kir} were less prevalent in striola than extrastriola, and, when present, the combined inward current was smaller (**Suppl. Fig. 6B**).

Discussion

We have shown that constitutive knockout of $K_V1.8$ eliminated $g_{K,L}$ in type I HCs, and g_A and much of g_{DR} in type II HCs. $K_V1.8$ immunolocalized specifically to the basolateral membranes of type I and II HCs. We conclude that $K_V1.8$ is a pore-forming subunit of $g_{K,L}$, g_A, and part of g_{DR} [$g_{DR}(K_V1.8)$]. We suggest that fast inactivation of g_A may arise from heteromultimerization of non-inactivating $K_V1.8$ subunits and inactivating $K_V1.4$ subunits. Finally, we showed that a substantial component of the residual delayed rectifier current in both type I and type II HCs comprises K_V7 channels.

$K_V1.8$ is expressed in hair cells from mammalian cochlea (Dierich et al., 2020), avian utricle (Scheibinger et al., 2022), and zebrafish (Erickson and Nicolson, 2015). Our work suggests that in anamniotes, which lack type I cells and $g_{K,L}$, $K_V1.8$ contributes to g_A and g_{DR}, which are widespread in vertebrate HCs (reviewed in Meredith and Rennie, 2016). $K_V1.8$ expression has not been detected in rodent brain but is reported in the pacemaker nucleus of weakly electric fish (Smith et al., 2018).

KV1.8 subunits may form homomultimers to produce gK,L in type I hair cells

Recent single-cell expression studies on mouse utricles (McInturff et al., 2018; Jan et al., 2021; Orvis et al., 2021) have detected just one K_V1 subunit, $K_V1.8$, in mouse type I HCs. Given that $K_V1.8$ can only form multimers with K_V1 family members, and given that $g_{K,L}$ channels are present at very high density (~150 per μm^2 in rat type I, Chen and Eatock, 2000), it stands to reason that most or all of the channels are $K_V1.8$ homomers. Other evidence is consistent with this proposal. $g_{K,L}$ (Rüsch and Eatock, 1996a) and heterologously expressed $K_V1.8$ homomers in oocytes (Lang et al., 2000) are non-inactivating and blocked by millimolar Ba^{2+} and 4-aminopyridine and >10 mM TEA. Unlike channels with $K_V1.1$, $K_V1.2$, and $K_V1.6$ subunits, $g_{K,L}$ is not sensitive to 10 nM α-dendrotoxin (Rüsch and Eatock, 1996a). $g_{K,L}$ and heterologously expressed $K_V1.8$ channels have similar single-channel conductances (~20 pS for $g_{K,L}$ at positive potentials, Chen and Eatock, 2000; 11 pS in oocytes, Lang et al., 2000). $g_{K,L}$ is inhibited—or positively voltage-shifted— by cGMP (Behrend et al., 1997; Chen and Eatock, 2000), presumably via the C-terminal cyclic nucleotide binding domain of $K_V1.8$.

A major novel property of $g_{K,L}$ is that it activates 30-60 mV negative to type II $K_V1.8$ conductances and most other low-voltage-activated K_V channels (Ranjan et al., 2019). The very negative activation range is a striking difference between $g_{K,L}$ and known homomeric $K_V1.8$ channels. Heterologously expressed homomeric $K_V1.8$ channels have an activation V_{half} of –10 to 0 mV (*X.*

laevis oocytes, Lang et al., 2000; CHO cells, Dierich et al., 2020). In cochlear inner HCs, currents attributed to $K_V1.8$ (by subtraction of other candidates) have a near-zero activation V_{half} (–4 mV, Dierich et al., 2020).

Possible factors in the unusually negative voltage dependence of $g_{K,L}$ include:

1. *elevation of extracellular K^+* by the enveloping calyceal terminal, unique to type I HCs (Lim et al., 2011; Contini et al., 2012; Spaiardi et al., 2020; Govindaraju et al., 2023). High K^+ increases conductance though $g_{K,L}$ channels (Contini et al., 2020), perhaps through K^+-mediated relief of C-type inactivation (López-Barneo et al., 1993; Baukrowitz and Yellen, 1995). We note, however, that $g_{K,L}$ is open at rest even in neonatal mouse utricles cultured without innervation (Rüsch et al., 1998) and persists in dissociated type I HCs (Chen and Eatock, 2000; Hurley et al., 2006).
2. *The high density of $g_{K,L}$* (~50 nS/pF in striolar $K_V1.8^{+/+}$ HCs) implies close packing of channels, possibly represented by particles (12-14 nm) seen in freeze-fracture electron microscopy of the type I HC membrane (Gulley and Bagger-Sjöbäck, 1979; Sousa et al., 2009). Such close channel packing might hyperpolarize *in situ* voltage dependence of $g_{K,L}$, as proposed for $K_V7.4$ channels in outer hair cells (Perez- Flores et al., 2020). Type I HC-specific partners that may facilitate this close packing include ADAM11 (McInturff et al., 2018), which clusters presynaptic $K_V1.1$ and $K_V1.2$ to enable ephaptic coupling at a cerebellar synapse (Kole et al., 2015).
3. *Modulation by accessory subunits*. Type I HCs express $K_V\beta1$ (McInturff et al., 2018; Orvis et al., 2021), an accessory subunit that can confer fast inactivation and hyperpolarize activation V_{half} by ~10 mV. $K_V\beta1$ might interact with $K_V1.8$ to shift voltage dependence negatively. Arguments against this possibility include that $g_{K,L}$ lacks fast inactivation (Rüsch and Eatock, 1996a; Hurley et al., 2006; Spaiardi et al., 2017) and that cochlear inner hair cells co-express $K_V1.8$ and $K_V\beta1$ (Liu et al., 2018) but their $K_V1.8$ conductance has a near-0 V_{half} (Dierich et al., 2020).

KV1.8 subunits may heteromerize with variable numbers of inactivating KV1.4 subunits to produce gA and KV1.8-dependent gDR in type II HCs

The $K_V1.8$-dependent conductances of type II HCs vary in their fast and slow inactivation. In not showing fast inactivation (Lang et al., 2000; Ranjan et al., 2019; Dierich et al., 2020), heterologously expressed $K_V1.8$ subunits resemble most other K_V1 family subunits, with the exception of $K_V1.4$ (for comprehensive review, see Ranjan et al., 2019). $K_V1.4$ is a good candidate to provide fast inactivation based on immunolocalization and voltage dependence (**Figs. 4**, **6**). We suggest that g_A and g_{DR}($K_V1.8$) are $K_V1.8$-containing channels that may include a variable number of $K_V1.4$ subunits and $K_V\beta2$ and $K_V\beta1$ accessory subunits.

$K_V1.4$-$K_V1.8$ heteromeric assembly could account for several related observations. The faster $\tau_{Inact,Fast}$ in $K_V1.8^{+/-}$ relative to $K_V1.8^{+/+}$ type II HCs (**Fig. 3A.3**, **Suppl. Fig. 2A.1**) could reflect an increased ratio of $K_V1.4$ to $K_V1.8$ subunits and therefore more N-terminal inactivation domains per heteromeric channel. Zonal variation in the extent and speed of N-type inactivation (**Fig. 3A**) might arise from differential expression of $K_V1.4$. The small fast-inactivating conductance in ~20% of extrastriolar $K_V1.8^{-/-}$ type II HCs (**Suppl. Fig. 4**) might flow through $K_V1.4$ homomers.

Fast inactivation may also receive contribution from $K_V\beta$ subunits. $K_V\beta1$ is expressed in type II HCs (McInturff et al., 2018; Jan et al., 2021; Orvis et al., 2021), and, together with $K_V1.4$, has been linked to g_A in pigeon vestibular HCs (Correia et al., 2008). $K_V\beta2$, also expressed in type II HCs (McInturff et al., 2018; Orvis et al., 2021), does not confer fast inactivation.

We speculate that g_A and $g_{DR}(K_V1.8)$ have different subunit composition: g_A may include heteromers of $K_V1.8$ with other subunits that confer rapid inactivation, while $g_{DR}(K_V1.8)$ may comprise homomeric $K_V1.8$ channels, given that they do not have N-type inactivation.

KV1.8 relevance for vestibular function

In both type I and type II utricular HCs, $K_V1.8$-dependent channels strongly shape receptor potentials in ways that promote temporal fidelity rather than electrical tuning (Lewis, 1988), consistent with the utricle's role in driving reflexes that compensate for head motions as they occur. This effect is especially pronounced for type I HCs, where the current-step evoked voltage response reproduces the input with great speed and linearity (**Fig. 2**).

$g_{K,L}$ dominates passive membrane properties in mature $K_V1.8^{+/+,+/-}$ type I HCs such that $K_V1.8^{-/-}$ type I HCs are expected to have receptor potentials with higher amplitudes but lower low-pass corner frequencies, closer to those of type II HCs and immature HCs of all types (Correia et al., 1996; Rüsch and Eatock, 1996a; Songer and Eatock, 2013). In $K_V1.8^{-/-}$ epithelia, we expect the lack of a large basolateral conductance open at rest to reduce the speed and gain of non-quantal transmission, which depends on K^+ ion efflux from the type I HC to change electrical and K^+ potentials in the synaptic cleft (Govindaraju et al., 2023). In hair cells, K^+ enters the mechanosensitive channels of the hair bundle from the K^+-rich apical endolymph and exits through basolateral potassium conductances into the more conventional low-K+ perilymph. For the type I-calyx synapse, having in the hair cell a large, non-inactivating K^+ conductance open across the physiological range of potentials avoids channel gating time and allows for instantaneous changes in current into the cleft and fast afferent signaling (Pastras et al., 2023).

In contrast, mature type II HCs face smaller synaptic contacts and have $K_V1.8$-dependent currents that are not substantially activated at resting potential. They do affect the time course and gain of type II HC responses to input currents, speeding up depolarizing transients, producing a repolarizing rebound during the step, and reducing resonance.

Type I and II vestibular hair cells are closely related, such that adult type II HCs acquire type I-like properties upon deletion of the transcription factor Sox2 (Stone et al., 2021). In normal development of the two cell types, the Kcna10 gene generates biophysically distinct and functionally different ion channels, presenting a natural experiment in functional differentiation of sensory receptor cells.

Materials and methods

Preparation

All procedures for handling animals followed the NIH Guide for the Care and Use of Laboratory Animals and were approved by the Institutional Animal Care and Use Committees of the University of Chicago and the University of Illinois Chicago. Most mice belonged to a transgenic line with a knockout allele of *Kcna10* (referred to here as $K_V1.8^{-/-}$). Our breeding colony was established with a generous gift of such animals from Sherry M. Jones and Thomas Friedman. These animals are described in their paper (Lee et al., 2013). Briefly, the Texas A&M Institute for Genomic Medicine generated the line on a C57BL/6;129SvEv mixed background by replacing Exon 3 of the *Kcna10* gene with an IRES-bGeo/Purocassette. Mice in our colony were raised on a 12:12h light-dark cycle with access to food and water *ad libitum*.

Semi-intact utricles were prepared from ~150 male and ~120 female mice, postnatal days (P) 5-375, for same-day recording. Hair cell K_V channel data were pooled across sexes as most results did not appear to differ by sex; an exception was that $g_{K,L}$ had a more negative V_{half} in males

(**Suppl. Table 1**), an effect not clearly related to age, copy number, or other properties of the activation curve.

Preparation, stimulation, and recording methods followed our previously described methods for the mouse utricle (Vollrath and Eatock, 2003). Mice were anesthetized through isoflurane inhalation. After decapitation, each hemisphere was bathed in ice-cold, oxygenated Liebowitz-15 (L15) media. The temporal bone was removed, the labyrinth was cut to isolate the utricle, and the nerve was cut close to the utricle. The utricle was treated with proteinase XXIV (100 µg/mL, ~10 mins, 22°C) to facilitate removal of the otoconia and attached gel layer and mounted beneath two glass rods affixed at one end to a coverslip.

Electrophysiology

We used the HEKA Multiclamp EPC10 with Patchmaster acquisition software, filtered by the integrated HEKA filters: a 6-pole Bessel filter at 10 kHz and a second 4-pole Bessel filter at 5 kHz, and sampled at 10- 100 kHz. Recording electrodes were pulled (PC-100, Narishige) from soda lime glass (King's Precision Glass R-6) wrapped in paraffin to reduce pipette capacitance. Internal solution contained (in mM) 135 KCl, 0.5 $MgCl_2$, 3 MgATP, 5 HEPES, 5 EGTA, 0.1 $CaCl_2$, 0.1 Na-cAMP, 0.1 LiGTP, 5 $Na_2CreatinePO_4$ adjusted to pH 7.25 and ~280 mmol/kg by adding ~30 mM KOH. External solution was Liebowitz-15 media supplemented with 10 mM HEPES (pH 7.40, 310 ± 10 mmol/kg). Recording temperature was 22-25°C. Pipette capacitance and membrane capacitance transients were subtracted during recordings with Patchmaster software. Series resistance (8-12 MΩ) was measured after rupture and compensated 60-80% with the amplifier, to final values of ~2 MΩ. Potentials are corrected for remaining (uncompensated) series resistance and liquid junction potential of ~+4 mV, calculated with LJPCalc software (Marino et al., 2014).

$K_V1.8^{-/-}$ hair cells appeared healthy in that cells had resting potentials negative to –50 mV, cells lasted a long time (20-30 minutes) in ruptured patch recordings, membranes were not fragile, and extensive blebbing was not seen. Type I HCs with $g_{K,L}$ were transiently hyperpolarized to –90 mV to close $g_{K,L}$ enough to increase R_{input} above 100 MΩ, as needed to estimate series resistance and cell capacitance. The average resting potential, V_{rest}, was –87 mV ± 1 (41), similar to the calculated E_K of –86.1 mV, which is not surprising given the large K^+ conductance of these cells. V_{rest} is likely more positive *in vivo*, where lower endolymphatic Ca^{2+} increases standing inward current through MET channels.

Voltage protocols to characterize K_V currents differed slightly for type I and II HCs. In standard protocols, the cell is held at a voltage near resting potential (–74 mV in type I and –64 mV in type II), then jumped to –124 mV for 200 ms in type I HCs in order to fully deactivate $g_{K,L}$ and 50 ms in type II HCs in order to remove baseline inactivation of g_A. The subsequent iterated step depolarizations lasted 500 ms in type I HCs because $g_{K,L}$ activates slowly (Wong et al., 2004) and 200 ms in type II HCs, where K_V conductances activate faster. The 50-ms tail voltage was near the reversal potential of HCN channels (–44 mV in mouse utricular hair cells, Rüsch et al., 1998) to avoid HCN current contamination.

G-V (activation) parameters for control type I cells may be expected to vary across experiments on semi-intact (as here), organotypically cultured and denervated (Rüsch et al.,1998), or dissociated-cell preparations, reflecting variation in retention of the calyx (Discussion) and voltage step durations (Wong et al., 2004) which elevate K^+ concentration around the hair cell. Nevertheless, the values we obtained for type I and type II HCs resemble values recorded elsewhere, including experiments in which extra care was taken to avoid extracellular K^+ accumulation (Spaiardi et al., 2017, 2020). The effects of K^+ accumulation on $g_{K,L}$'s steady-state activation curves are small because the operating range is centered on E_K and can be characterized with relatively small currents (**Fig. 1A**).

Pharmacology

Drug-containing solutions were locally with BASI Bee Hive syringes at a final flow rate of 20 µL/min and a dead time of ~30 s. Global bath perfusion was paused during drug perfusion and recording, and only one cell was used per utricle. Aliquots of test agents in solution were prepared, stored at –20°C, and thawed and added to external solution on the recording day (see **Key Resources Table**).

Analysis

Data analysis was performed with software from OriginLab (Northampton, MA) and custom MATLAB scripts using MATLAB fitting algorithms.

Fitting voltage dependence and time course of conductances

G-V curves. Current was converted to conductance (G) by dividing by driving force ($V - E_K$; E_K calculated from solutions). For type I HCs, tail G-V curves were generated from current 1 ms after the end of the iterated voltage test step. For type II HCs, peak G-V curves were generated from peak current during the step and steady-state G-V curves were generated from current 1 ms before the end of a 200 ms step. Sigmoidal voltage dependence of G-V curves was fit with the first-order Boltzmann equation (**Eq. 1**).

$$G(V) = G_{min} + \frac{G_{max}}{1 + e^{\frac{V_{half} - V}{S}}} \quad (1)$$

V_{half} is the midpoint and S is the slope factor, inversely related to curve steepness near activation threshold.

Activation time course of type II HCs. For type II HCs lacking fast inactivation, outward current activation was fit with **Eq. 2**.

$$I(t) = I_{SS} * \left(1 - e^{-\frac{t}{\tau_w}}\right)^n + I_0 \quad (2)$$

I_{SS} is steady-state current, τ_w is activation time constant, n is the state factor related to the number of closed states (typically constrained to 3), and I_0 is baseline current.

To measure activation and inactivation time course of g_A, we used **Eq. 3** to fit outward K^+ currents evoked by steps from –125 mV to above –50 mV (Rothman and Manis, 2003b).

$$I(t) = I_{max} * \left(1 - e^{-\frac{t}{\tau_w}}\right)^n * (1 - Z * (f * \left(1 - e^{-\frac{t}{\tau_{zf}}}\right) + (1 - f) * \left(1 - e^{-\frac{t}{\tau_{zs}}}\right)) + I_0 \quad (3)$$

Z is total steady-state inactivation ($0 \le Z < 1$ means incomplete inactivation, which allows the equation to fit non-inactivating delayed rectifier currents), f is the fraction of fast inactivation relative to total inactivation, I_{max} is maximal current, τ_{zf} and τ_{zs} are the fast and slow inactivation time constants. We chose to compare fit parameters at 30 ± 2 mV (91), where fast and slow inactivation were consistently separable and g_A was maximized. In most $K_V1.8^{-/-}$ and some striolar $K_V1.8^{+/+,+/-}$ cells, where fast inactivation was absent and adjusted R^2 did not improve on a single-exponential fit by >0.01, we constrained f in Eq. 3 to 0 to avoid overfitting.

For *Peak* G-V relations, peak conductance was taken from fitted curves (Eqs. 2 and 3). To construct '*Steady-state*' G-V relations, we used current at 200 ms (6 ± 1 % (94) greater than steady-state estimated from fits to Eq. 3 (**Fig. 3C-D**)).

Percent inactivation was calculated at 30 mV with **Eq. 4** :

$$\%\ Inactivation = (I_{Peak} - I_{SS})/I_{Peak} \quad (4)$$

I_{Peak} is maximal current, and I_{SS} is current at the end of a 200 ms voltage step.

The electrical resonance of type II HCs was quantified by fitting voltage responses to current injection steps (Songer and Eatock, 2013). We fit Eq. 5, a damped sinusoid, to the voltage trace from half-maximum of the initial depolarizing peak until the end of the current step.

$$V(t) = V_{ss} + V_p * e^{-\frac{t}{\tau_e}} * \sin(2\pi f_e - \theta) \quad (5)$$

V_{SS} is steady-state voltage, V_p is the voltage of the peak response, τ_e is the decay time constant, f_e is the fundamental frequency, and θ is the phase angle shift.

Quality factor, Q_e, was calculated with Eq. 6 (Crawford and Fettiplace, 1981).

$$Q_e = [(\pi f_e \tau_e)^2 + 0.25]^{1/2} \quad (6)$$

Statistics

We give means ± SEM for normally-distributed data, and otherwise, median and range. Data normality was assessed with the Shapiro-Wilk test for n50. To assess homogeneity of variance we used Levene's test. With homogeneous variance, we used two-way ANOVA for genotype and zone with the posthoc Tukey's test. When variance was non-homogeneous, we used one-way Welch ANOVA with the posthoc Games-Howell test. For data that were not normally distributed, we used the non-parametric one-way Kruskal-Wallis ANOVA (KWA) with posthoc Dunn's test. Effect size is Hedge's g (g). For age dependence, we used partial correlation coefficients controlling for genotype and zone. Statistical groups may have different median ages, but all have overlapping age ranges. In figures, asterisks represent p-value ranges as follows: *, p<0.05; **, p<0.01; ***, p<0.001; ****, p<0.0001.

Immunohistochemistry

Mice were anesthetized with Nembutal (80 mg/kg), then perfused transcardially with 40mL of physiological saline containing heparin (400 IU), followed by 2 mL/g body weight fixative (4% paraformaldehyde, 1% picric acid, and 5% sucrose in 0.1 M phosphate buffer at pH 7.4, sometimes with 1% acrolein). Vestibular epithelia were dissected in phosphate buffer, and tissues were cryoprotected in 30% sucrose-phosphate buffer overnight at 4°C. Otoconia were dissolved with Cal-Ex (Fisher Scientific) for 10 min. Frozen sections (35 µm) were cut with a sliding microtome. Immunohistochemistry was performed on free-floating sections. Tissues were first permeabilized with 4% Triton X-100 in PBS for 1 h at room temperature, then incubated with 0.5% Triton X-100 in a blocking solution of 0.5% fish gelatin and 1% BSA for 1 h at room temperature. Sections were incubated with 2-3 primary antibodies for 72 h at 4°C and with 2-3 secondary antibodies. Sections were rinsed with PBS between and after incubations and mounted on slides in Mowiol (Calbiochem).

Data Availability

Data used in this study are available on Dryad (*https://doi.org/10.5061/dryad.37pvmcvrw*).

Acknowledgements

This study was supported by NIH grant R01 DC012347 to RAE and AL and an NSF Graduate Research Fellowship to HRM. We thank Drs. Thomas Friedman and Sherri Jones for the generous gift of the $K_V1.8^{-/-}$ mouse line, and Drs. Zheng-Yi Chen and Deborah I. Scheffer for bringing the expression of this subunit in mouse vestibular hair cells to our attention.

We acknowledge Dr. Vicente Lumbreras for insights from his prior experiments on g_A in mouse utricular hair cells, and thank him for helpful further discussions.

We acknowledge Steven D. Price for his help with immunocytochemistry.

We thank Drs. Rebecca Lim and Ebenezer Yamoah for their critical feedback on the manuscript, and Drs. Rob Raphael and Aravind Chenrayan Govindaraju for feedback and many helpful discussions. We thank Drs. Joe Burns, Gabi Pregernig, and Lars Becker (Decibel Therapeutics, Inc.) for helpful discussions.

Author Contributions

HRM designed and performed experiments, analyzed data, and wrote the paper; RAE helped design experiments, analyze data, and write the paper; AL performed immunohistochemistry experiments and reviewed and edited the manuscript.

Abbreviations

- g_A: A-type (inactivating) K_V conductance in type II HCs g_{DR}, delayed rectifier K^+ conductance
- $g_{K,L}$: low-voltage-activated K^+ conductance in type I HCs
- HC: hair cell
- K_V: voltage-gated K^+ conductance

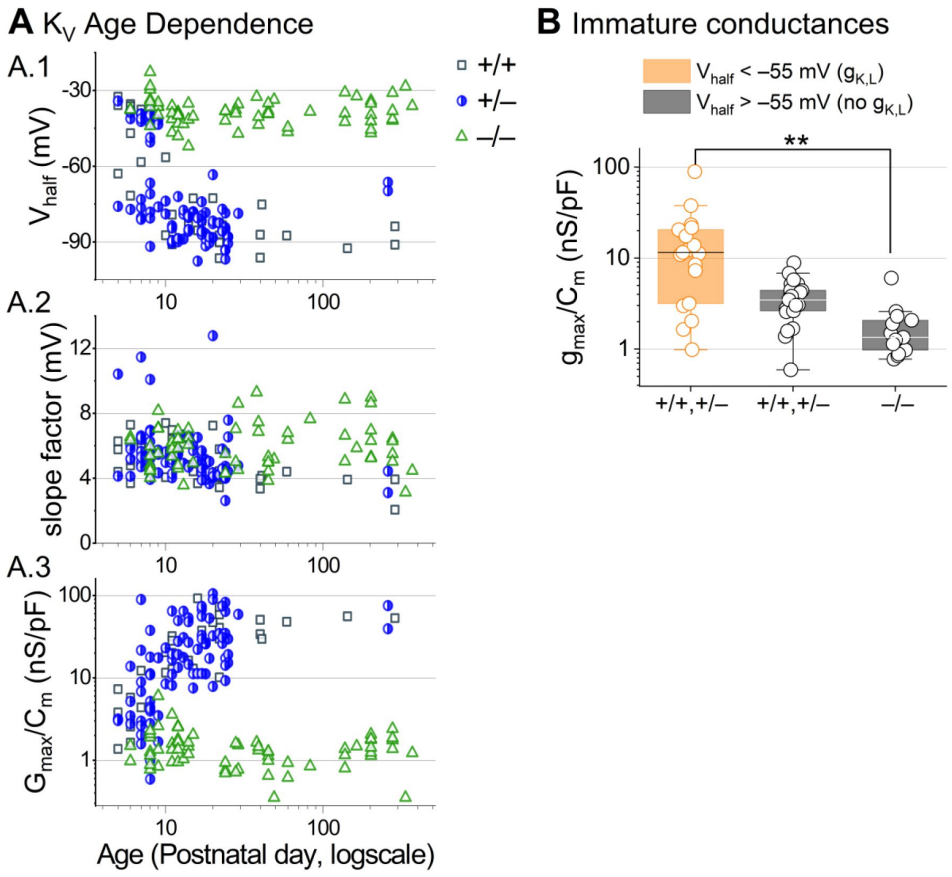

Supplemental Figure 1.

Developmental changes in type I HC K_V conductances.

(A) Parameters from Boltzmann fits of tail G-V relations for type I HCs plotted against age.

(B) Conductance density is similar in young (P5-P10) type I HCs that lack $g_{K,L}$. $g_{K,L}$ is defined here as having a V_{half} negative to –55 mV. $K_V1.8^{+/+,+/-}$ *with* $g_{K,L}$, 17 ± 5 nS/pF (19); $K_V1.8^{+/+,+/-}$ *without* $g_{K,L}$, 3.7 ± 0.4 nS/pF (22); $K_V1.8^{-/-}$, 1.8 ± 0.4 nS/pF (13). $K_V1.8^{+/+,+/-}$ *with* $g_{K,L}$ vs. $K_V1.8^{-/-}$: p = 0.007, KWA, g 1.0.

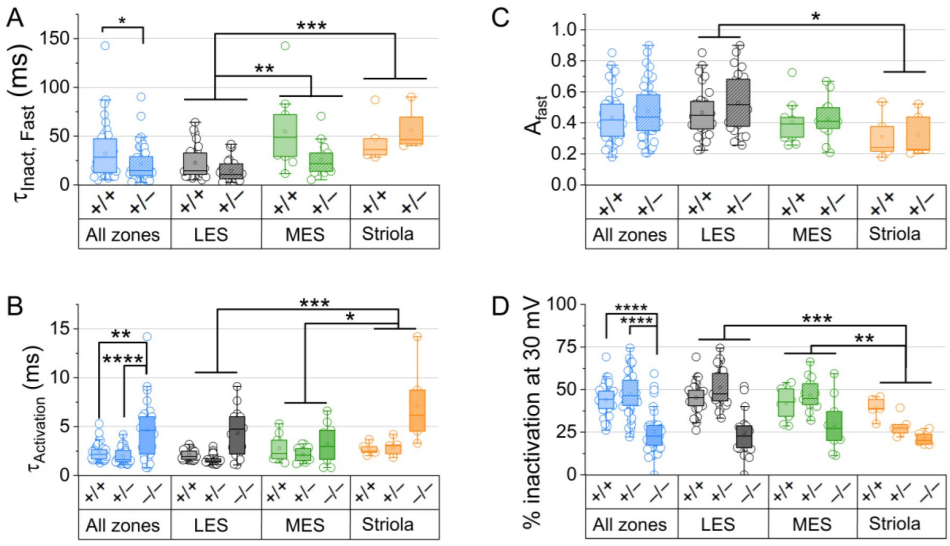

Supplemental Figure 2.

For type II HCs older than P12, K_V conductance activation and inactivation differed across zones and genotypes.
(A) $\tau_{inact,Fast}$ at 30 mV was fastest in LES in $K_V1.8^{+/+}$ and $K_V1.8^{+/-}$ HCs, and faster in $K_V1.8^{+/-}$ than $K_V1.8^{+/+}$ HCs (see **Table 3** for p-values).
(B) Fast inactivation was a larger fraction of the total in LES than striola.
(C) τ_{Act} at 30 mV was slower in $K_V1.8^{-/-}$ than $K_V1.8^{+/+}$ and $K_V1.8^{+/-}$, and slower in striola than LES and MES.
(D) Percent inactivation at 30 mV was lowest in striola (zone effect), and lowest in $K_V1.8^{-/-}$ HCs (genotype effect).

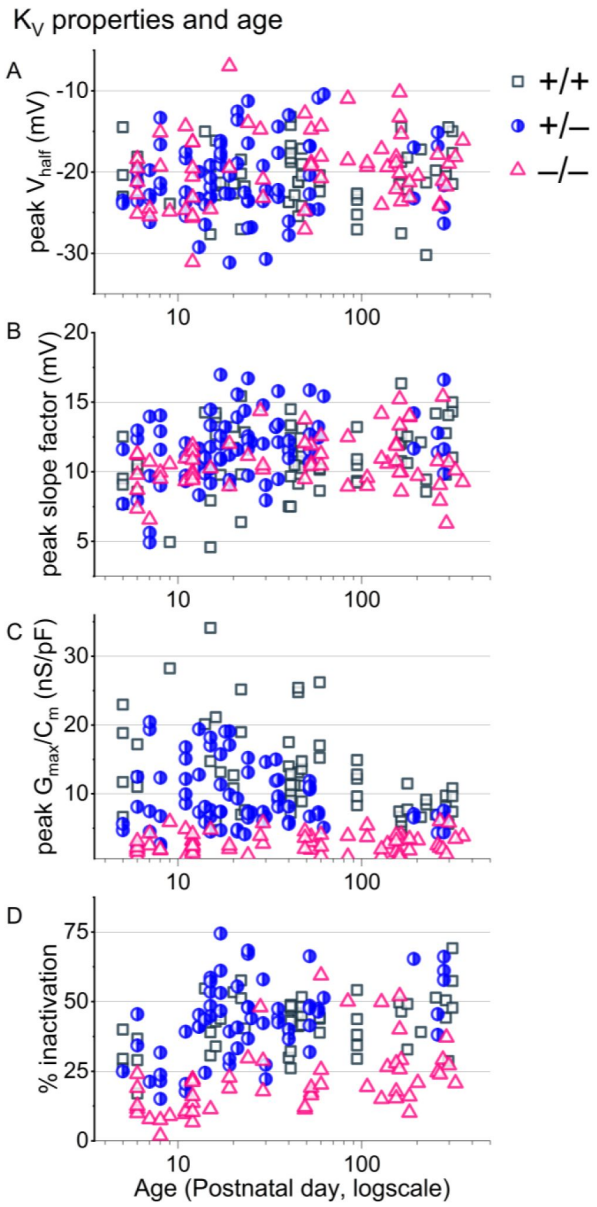

Supplemental Figure 3.

For type II HCs older than P12, K_V conductances were stable.
(**A-C**) Parameters from Boltzmann fits of peak G-V relations and (**D**) % inactivation at +30 mV plotted against age from all zones. Overlaid curves are smoothing cubic β-splines. Note the seven extrastriolar $K_V1.8^{-/-}$ type II HCs with % inactivation >30%.

Supplemental Figure 4.

A minority of extrastriolar $K_V1.8^{-/-}$ type II HCs had a very small fast- inactivating outward rectifier current.

(A) All extrastriolar $K_V1.8^{+/+,+/-}$ type II HCs inactivated by >30%. Most mature (>P12) extrastriolar $K_V1.8^{-/-}$ type II HCs inactivated by <30% but some inactivated by >30% (7/30, 23%) because they had fast inactivation (B).
(B) Exemplar residual fast inactivation ($\tau_{FastInact}$ = 10 ms at +30 mV). For the 7 cells in this group, $\tau_{FastInact}$= 30 ± 6 ms, amplitude of fast inactivation = 310 ± 70 pA; activation peak V_{half} = −15 ± 2 mV and slope factor = 12.4 ± 0.9 mV. These parameters are similar to g_A but for the much smaller conductance (one- way ANOVAs).

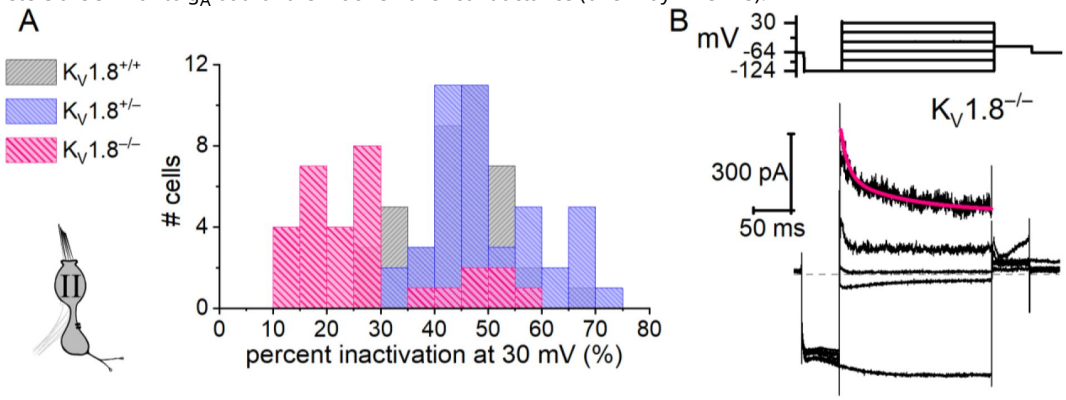

Supplemental Figure 5.

A minority of striolar $K_V1.8^{-/-}$ type I HCs had a small low-voltage-activated outward rectifier current in addition to a more positively activating outward rectifier.

(**A**) Low-voltage-activated current from one cell was isolated by subtraction with 10 µM XE991 (P39), indicating that it was carried by K_V7 channels. Deactivation of XE991-sensitive current evoked by step from −64 mV to −124 mV *(arrow)* was fit with exponential decay (τ = 21 ms). (**B**) XE991-sensitive tail G-V curve of the XE991-blocked conductance (A) was fit with a sum of two Boltzmann equations: $G(V) = A_1/(1 + \exp((V_{half,1} - V)/S_1)) + A_2/(1 + \exp((V_{half,2} - V)/S_2))$.
(**C**) The low-voltage-activated $V_{half,1}$ component was only seen in striolar $K_V1.8^{-/-}$ type I HCs, and even there in the minority: 5/23; 22%; P6-P370). It was always seen together with a more positively activating outward rectifier. Boltzmann parameters, including (B): $A_1/(A_1+A_2)$ = 0.15 ± 0.04, $V_{half,1}$ = −106 ± 5 mV (n=5), S_1 = 3.8 ± 0.8 mV, $V_{half,2}$ = −41 ± 1 mV, S_2 = 7 ± 1 mV. Ages: P11, 39, 202, 202, 202. No extrastriolar type I HCs (0/45; P6-277) had a double activation tail G-V curve.

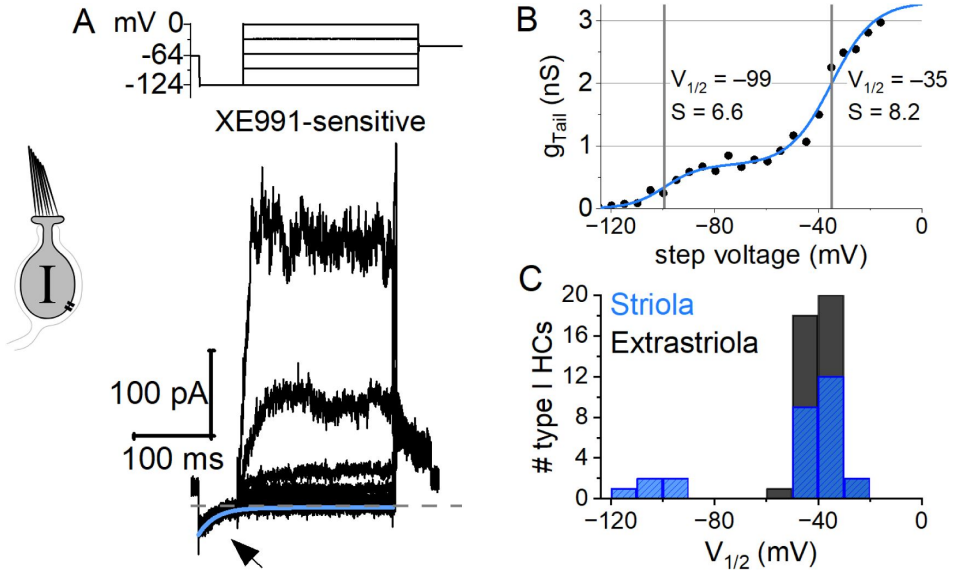

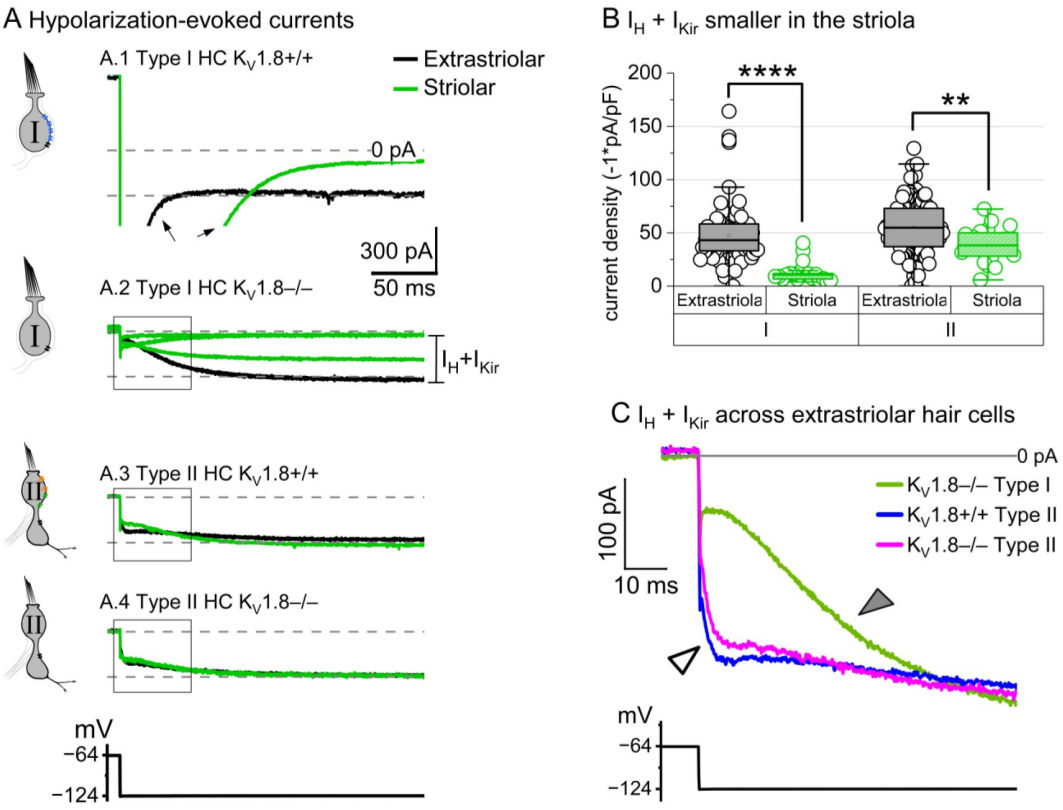

Supplemental Figure 6.

No difference was detected in H (HCN) and Kir (fast inward rectifier) currents between $K_V1.8^{+/+}$ and $K_V1.8^{-/-}$ hair cells, consistent with a specific involvement of K_V1.8 in *Kcna10* expression.

(A) Hyperpolarizing voltage steps evoked I_{Kir} and I_{HCN} in $K_V1.8^{+/+,+/-,-/-}$ type I and II HCs. **A.1** *Arrows*, deactivation of $g_{K,L}$. **A.2-A.4** *Bracket,* the sum of I_H and I_{Kir} were measured as total inward current after 250 ms at –124 mV.
(B) Summed I_{KIR} and I_H density was the same across genotypes but smaller in striola than extrastriola (see **Supplemental Table 3** for statistics).
(C) Inward currents seen at the onset of hyperpolarization, including I_{Kir}, were larger in type II HCs than type I. Magnification of boxed in inset from the extrastriolar cells in A.2-A.4. *Open arrowhead*, activation of fast inward rectifier, I_{Kir}; *filled arrowhead*, slower activation of I_{HCN}.

Supplemental Table 1.

Test of sex differences in hair cell K_V channel data.

Cell Type	Parameter	Subgroup	Male vs Female posthoc p-value	Test
Type I HC	Tail V_{half}	+/+,+/– –/–	0.0023 ** [a] 0.57	Normal, homogeneous variance ANOVA: Genotype (2 levels), Sex (2 levels), Zone (2 levels), Genotype*Sex.
	Tail S	+/+,+/– –/–	0.98 0.58	ANOVA: Genotype (2 levels), Sex (2 levels), Zone (2 levels), Genotype*Sex. Normal, homogeneous variance
	Tail $g_{Density}$	+/+,+/– –/–	0.999 0.936	Normal, nonhomogeneous variance Welch ANOVA: Genotype*Sex
Type II HC	Peak V_{half}	+/+,+/– –/–	0.95 0.28	Normal, homogeneous variance ANOVA: Genotype (2 levels), Sex (2 levels), Zone (2 levels), Genotype*Sex.
	Peak S	+/+,+/– –/–	0.999 0.97	Normal, homogeneous variance ANOVA: Genotype (2 levels), Sex (2 levels), Zone (2 levels), Genotype*Sex.
	Peak $g_{Density}$	+/+,+/– –/–	0.64 0.43	Normal, nonhomogeneous variance Welch ANOVA: Genotype*Sex
	% inactivation at 30 mV	+/+,+/– –/–	0.98 0.82	Normal, homogeneous variance ANOVA: Genotype (2 levels), Sex (2 levels), Zone (2 levels), Genotype*Sex.

[a] g, 0.9. Male $K_V1.8^{+/+,+/-}$, –85 ± 1 mV (40) vs. Female $K_V1.8^{+/+,+/-}$, –79 ± 2 mV (12)

Supplemental Table 2.

Soma size of type I HCs. The perimeter of cross-sections of basolateral cell bodies was manually measured from immunohistochemistry sections with sufficient autofluorescence in the 488 channel to distinguish cell morphology, and anti-calretinin to label type II hair cells and calyx-only afferents. Cells were measured from two female littermates.

Cell Type	Genotype	Age	Weight (g)	Perimeter (μm)	Test
Type I HC	+/+ –/–	P117 P117	24.9 25.2	47 ± 1 (19) 46 ± 1 (28)	ANOVA: p=0.1, power = 0.07

Cell Type	Zone	I_H + I_{Kir} current density (-1*pA/pF)	$K_v1.8^{+/+,+/-}$ *vs* $K_v1.8^{-/-}$ p-value	ES *vs* Striola p-value	Test
Type I HC	ES Striola	48 ± 3 (78) 13.0 ± 2 (19)	0.3	4E-9 **** [a]	Non-normal, KWA
Type II HC	ES Striola	55 ± 2 (116) 39 ± 4 (20)	0.19 (0.25 power)	0.0058 ** [b]	Normal, homogeneous variance. 2-way ANOVA: Genotype (2 levels), Zone (2 levels)

[a] g 1.4
[b] g 0.6

Supplemental Table 3.

Detected zonal but not genotype differences in hair cell I_{Kir} and I_H.

References

1. Alexander SPH, et al. (2019) **The Concise Guide to Pharmacology 2019/20: Ion channels**

2. Al-Sabi A, Kaza S, Le Berre M, O'Hara L, Bodeker M, Wang J, Dolly JO (2011) **Position-dependent attenuation by Kv1.6 of N-type inactivation of Kv1.4-containing channels** *Biochem J* **438**:389–396

3. Ashmore JF (1983) **Frequency tuning in a frog vestibular organ** *Nature* **304**:536–538

4. Bao H, Wong WH, Goldberg JM, Eatock RA (2003) **Voltage-Gated Calcium Channel Currents in Type I and Type II Hair Cells Isolated From the Rat Crista** *J Neurophysiol* **90**:155–164

5. Baukrowitz T, Yellen G (1995) **Modulation of K+ current by frequency and external [K+]: A tale of two inactivation mechanisms** *Neuron* **15**:951–960

6. Behrend O, Schwark C, Kunihiro T, Strupp M (1997) **Cyclic GMP inhibits and shifts the activation curve of the delayed rectifier (I(K1)) of type I mammalian vestibular hair cells** *NeuroReport* **8**:2687–2690

7. Brown DA, Selyanko AA, Hadley JK, Tatulian L (2002) **Some Pharmacological Properties Of Neural KCNQ Channels** *Neurophysiology* **34**:91–94

8. Carlisle FA, Steel KP, Lewis MA (2012) **Specific expression of Kcna10** *Pxn and Odf2 in the organ of Corti. Gene Expression Patterns* **12**:172–179

9. Chen JWY, Eatock RA (2000) **Major Potassium Conductance in Type I Hair Cells from Rat Semicircular Canals: Characterization and Modulation by Nitric Oxide** *J Neurophysiol* **84**:139–151

10. Contini D, Holstein GR, Art JJ (2020) **Synaptic cleft microenvironment influences potassium permeation and synaptic transmission in hair cells surrounded by calyx afferents in the turtle** *J Physiol* **598**:853–889

11. Contini D, Price SD, Art JJ (2017) **Accumulation of K+ in the synaptic cleft modulates activity by influencing both vestibular hair cell and calyx afferent in the turtle: K+ modulation of synaptic transmission between hair cell and afferent** *J Physiol* **595**:777–803

12. Contini D, Zampini V, Tavazzani E, Magistretti J, Russo G, Prigioni I, Masetto S (2012) **Intercellular K+ accumulation depolarizes Type I vestibular hair cells and their associated afferent nerve calyx** *Neuroscience* **227**:232–246

13. Correia MJ, Lang DG (1990) **An electrophysiological comparison of solitary type I and type II vestibular hair cells** *Neuroscience Letters* **116**:106–111

14. Correia MJ, Ricci AJ, Rennie KJ (1996) **Filtering Properties of Vestibular Hair Cells: An Update** *Ann NY Acad Sci* **781**:138–149

15. Correia MJ, Weng T, Prusak D, Wood TG (2008) **Kvβ1.1 Associates with Kv1.4 in Chinese Hamster Ovary Cells and Pigeon Type II Vestibular Hair Cells and Enhances the Amplitude, Inactivation and Negatively Shifts the Steady-State Inactivation Range** *Neuroscience* **152**:809–820

16. Crawford AC, Fettiplace R (1981) **An electrical tuning mechanism in turtle cochlear hair cells** *J Physiol* **312**:377–412

17. Desai SS, Zeh C, Lysakowski A (2005) **Comparative Morphology of Rodent Vestibular Periphery** *I. Saccular and Utricular Maculae. J Neurophysiol* **93**:251–266

18. Dierich M, Altoè A, Koppelmann J, Evers S, Renigunta V, Schäfer MK, Naumann R, Verhulst S, Oliver D, Leitner MG (2020) **Optimized Tuning of Auditory Inner Hair Cells to Encode Complex Sound through Synergistic Activity of Six Independent K+ Current Entities** *Cell Reports* **32**

19. Dwenger MM, Raph SM, Baba SP, Moore JB, Nystoriak MA (2022) **Diversification of Potassium Currents in Excitable Cells via Kvβ Proteins** *Cells* **11**

20. Eatock RA, Songer JE (2011) **Vestibular Hair Cells and Afferents: Two Channels for Head Motion Signals** *Annu Rev Neurosci* **34**:501–534

21. Erickson T, Nicolson T (2015) **Identification of sensory hair-cell transcripts by thiouracil-tagging in zebrafish** *BMC Genomics* **16**

22. Fettiplace R (1987) **Electrical tuning of hair cells in the inner ear** *TINS* **10**

23. Géléoc GS, Risner J, Holt JR (2004) **Developmental Acquisition of Voltage-Dependent Conductances and Sensory Signaling in Hair Cells of the Embryonic Mouse Inner Ear** *J Neurosci* **24**:11148–11159

24. Goldberg JM (2000) **Afferent diversity and the organization of central vestibular pathways** *Exp Brain Res* **130**:277–297

25. González-Garrido A, Pujol R, López-Ramírez O, Finkbeiner C, Eatock RA, Stone JS (2021) **The Differentiation Status of Hair Cells That Regenerate Naturally in the Vestibular Inner Ear of the Adult Mouse** *J Neurosci* **41**:7779–7796

26. Govindaraju AC, Quraishi IH, Lysakowski A, Eatock RA, Raphael RM (2023) **Nonquantal transmission at the vestibular hair cell–calyx synapse: KLV currents modulate fast electrical and slow K + potentials** *Proc Natl Acad Sci USA* **120**

27. Gulley A, Bagger-Sjöbäck D (1979) **Freeze-fracture studies on the synapse between the type I hair cells and the calyceal terminal in the guinea-pig vestibular system** *J Neurocytol* **8**:591–603

28. Holt JR, Stauffer EA, Abraham D, Geleoc GSG (2007) **Dominant-Negative Inhibition of M-Like Potassium Conductances in Hair Cells of the Mouse Inner Ear** *J Neurosci* **27**:8940–8951

29. Horwitz GC, Risner-Janiczek JR, Jones SM, Holt JR (2011) **HCN Channels Expressed in the Inner Ear Are Necessary for Normal Balance Function** *J Neurosci* **31**:16814–16825

30. Hudspeth AJ, Lewis RS (1988) **A model for electrical resonance and frequency tuning in saccular hair cells of the bull-frog, Rana catesbeiana** *J Physiol* **400**:275–297

31. Hurley KM, Gaboyard S, Zhong M, Price SD, Wooltorton JRA, Lysakowski A, Eatock RA (2006) **M-Like K+ Currents in Type I Hair Cells and Calyx Afferent Endings of the Developing Rat Utricle** *Journal of Neuroscience* **26**:10253–10269

32. Imbrici P, D'Adamo MC, Kullmann DM, Pessia M (2006) **Episodic ataxia type 1 mutations in the KCNA1 gene impair the fast inactivation properties of the human potassium channels Kv1.4-1.1/Kvβ1.1 and Kv1.4-1.1/Kvβ1.2** *Eur J Neurosci* **24**:3073–3083

33. Jan TA, Eltawil Y, Ling AH, Chen L, Ellwanger DC, Heller S, Cheng AG (2021) **Spatiotemporal dynamics of inner ear sensory and non-sensory cells revealed by single-cell transcriptomics** *Cell Reports* **36**

34. Jensen HS, Grunnet M, Olesen S-P (2007) **Inactivation as a New Regulatory Mechanism for Neuronal Kv7 Channels** *Biophys J* **92**:2747–2756

35. Kharkovets T, Hardelin J-P, Safieddine S, Schweizer M, El-Amraoui A, Petit C, Jentsch TJ (2000) **KCNQ4, a K+ channel mutated in a form of dominant deafness, is expressed in the inner ear and the central auditory pathway** *Proc Natl Acad Sci USA* **97**:4333–4338

36. Kole MJ, Qian J, Waase MP, Klassen TL, Chen TT, Augustine GJ, Noebels JL (2015) **Selective Loss of Presynaptic Potassium Channel Clusters at the Cerebellar Basket Cell Terminal Pinceau in Adam11 Mutants Reveals Their Role in Ephaptic Control of Purkinje Cell Firing** *J Neurosci* **35**:11433–11444

37. Kubisch C, Schroeder BC, Friedrich T, Lütjohann B, El-Amraoui A, Marlin S, Petit C, Jentsch TJ (1999) **KCNQ4, a Novel Potassium Channel Expressed in Sensory Outer Hair Cells, Is Mutated in Dominant Deafness** *Cell* **96**:437–446

38. Lang R, Lee G, Liu W, Tian S, Rafi H, Orias M, Segal AS, Desir GV (2000) **KCNA10: A novel ion channel functionally related to both voltage-gated potassium and CNG cation channels** *American Journal of Physiology - Renal Physiology* **278**

39. Lee SI, Conrad T, Jones SM, Lagziel A, Starost MF, Belyantseva IA, Friedman TB, Morell RJ (2013) **A null mutation of mouse Kcna10 causes significant vestibular and mild hearing dysfunction** *Hear Res* **300**:1–9

40. Levin ME, Holt JR (2012) **The function and molecular identity of inward rectifier channels in vestibular hair cells of the mouse inner ear** *J Neurophysiol* **108**:175–186

41. Lewis ER (1988) **Tuning in the bullfrog ear** *Biophysical Journal* **53**:441–447

42. Lim R, Kindig AE, Donne SW, Callister RJ, Brichta AM (2011) **Potassium accumulation between type I hair cells and calyx terminals in mouse crista** *Exp Brain Res* **210**:607–621

43. Liu H, Chen L, Giffen KP, Stringham ST, Li Y, Judge PD, Beisel KW, He DZZ (2018) **Cell-Specific Transcriptome Analysis Shows That Adult Pillar and Deiters' Cells Express Genes Encoding Machinery for Specializations of Cochlear Hair Cells** *Front Mol Neurosci* **11**

44. López-Barneo J, Hoshi T, Heinemann SH, Aldrich RW (1993) **Effects of external cations and mutations in the pore region on C-type inactivation of Shaker potassium channels** *Recept Channels* **1**:61–71

45. Lysakowski A, Gaboyard-Niay S, Calin-Jageman I, Chatlani S, Price SD, Eatock RA (2011) **Molecular Microdomains in a Sensory Terminal, the Vestibular Calyx Ending** *J Neurosci* **31**:10101–10114

46. Lysakowski A, Goldberg JM (2004) **Morphophysiology of the vestibular periphery** :57–152 https://doi.org/10.1007/0-387-21567-0_3

47. Marino M, Misuri L, Brogioli D (2014) **A new open source software for the calculation of the liquid junction potential between two solutions according to the stationary Nernst-Planck equation** *arXiv*

48. Masetto S, Correia MJ (1997) **Electrophysiological Properties of Vestibular Sensory and Supporting Cells in the Labyrinth Slice Before and During Regeneration** *J Neurophysiol* **78**:1913–1927

49. McInturff S, Burns JC, Kelley MW (2018) **Characterization of spatial and temporal development of Type I and Type II hair cells in the mouse utricle using new cell-type-specific markers** *Biol Open* **7**

50. Meredith FL, Rennie KJ (2016) **Channeling your inner ear potassium: K+ channels in vestibular hair cells** *Hear Res* **338**:40–51

51. Mitra K, Ubarretxena-Belandia I, Taguchi T, Warren G, Engelman DM (2004) **Modulation of the bilayer thickness of exocytic pathway membranes by membrane proteins rather than cholesterol** *Proc Natl Acad Sci USA* **101**:4083–4088

52. Orvis J, et al. (2021) **gEAR: Gene Expression Analysis Resource portal for community-driven, multi-omic data exploration** *Nat Methods* **18**:843–844

53. Pastras CJ, Curthoys IS, Asadnia M, McAlpine D, Rabbitt RD, Brown DJ (2023) **Evidence that ultrafast non- quantal transmission underlies synchronized vestibular action potential generation** *J Neurosci:JN-RM* :1417–23

54. Perez-Flores MC *et al.* (2020) **Cooperativity of K v 7.4 channels confers ultrafast electromechanical sensitivity and emergent properties in cochlear outer hair cells** *Sci Adv* **6**

55. Pujol R, Pickett SB, Nguyen TB, Stone JS (2014) **Large basolateral processes on type II hair cells are novel processing units in mammalian vestibular organs: Basolateral Processes of Type II Hair Cells** *J Comp Neurol* **522**:3141–3159

56. Ramanathan K, Fuchs PA (2002) **Modeling Hair Cell Tuning by Expression Gradients of Potassium Channel** *Biophys J* **82**:64–72

57. Ranjan R, Logette E, Marani M, Herzog M, Tache V, Scantamburlo E, Buchilier V, Markram H (2019) **A Kinetic Map of the Homomeric Voltage-Gated Potassium Channel (Kv) Family** *Front Cell Neurosci* **13**

58. Rennie KJ, Correia MJ (1994) **Potassium currents in mammalian and avian isolated type I semicircular canal hair cells** *J Neurophysiol* **71**:317–329

59. Rennie KJ, Weng T, Correia MJ (2001) **Effects of KCNQ channel blockers on K+ currents in vestibular hair cells** *Am J Physiol Cell Physiol* **280**:C473–C480

60. Ricci AJ, Rennie KJ, Correia MJ (1996) **The delayed rectifier** *IKI, is the major conductance in type I vestibular hair cells across vestibular end organs. Pflüg Arch Eur J Physiol* **432**:34–42

61. Rothman JS, Manis PB (2003) **Kinetic Analyses of Three Distinct Potassium Conductances in Ventral Cochlear Nucleus Neurons** *J Neurophysiol* **89**:3083–3096

62. Rüsch A, Eatock RA (1996) **A delayed rectifier conductance in type I hair cells of the mouse utricle** *J Neurophysiol* **76**:995–1004

63. Rüsch A, Eatock RA (1996) **Voltage Responses of Mouse Utricular Hair Cells to Injected Currents** *Ann NY Acad Sci* **781**:71–84

64. Rüsch A, Lysakowski A, Eatock RA (1998) **Postnatal development of type I and type II hair cells in the mouse utricle: Acquisition of voltage-gated conductances and differentiated morphology** *Journal of Neuroscience* **18**:7487–7501

65. Scheffer DI, Shen J, Corey DP, Chen Z-Y (2015) **Gene Expression by Mouse Inner Ear Hair Cells during Development** *J Neurosci* **35**:6366–6380

66. Scheibinger M, Janesick A, Benkafadar N, Ellwanger DC, Jan TA, Heller S (2022) **Cell-type identity of the avian utricle** *Cell Reports* **40**

67. Schroeder BC, Hechenberger M, Weinreich F, Kubisch C, Jentsch TJ (2000) **KCNQ5, a Novel Potassium Channel Broadly Expressed in Brain, Mediates M-type Currents** *Journal of Biological Chemistry* **275**:24089–24095

68. Schweizer FE, Savin D, Luu C, Sultemeier DR, Hoffman LF (2009) **Distribution of high-conductance calcium-activated potassium channels in rat vestibular epithelia** *J Comp Neurol* **517**:134–145

69. Smith GT, Proffitt MR, Smith AR, Rusch DB (2018) **Genes linked to species diversity in a sexually dimorphic communication signal in electric fish** *J Comp Physiol A* **204**:93–112

70. Songer JE, Eatock RA (2013) **Tuning and Timing in Mammalian Type I Hair Cells and Calyceal Synapses** *J Neurosci* **33**:3706–3724

71. Sousa AD, Andrade LR, Salles FT, Pillai AM, Buttermore ED, Bhat MA, Kachar B (2009) **The Septate Junction Protein Caspr Is Required for Structural Support and Retention of KCNQ4 at Calyceal Synapses of Vestibular Hair Cells** *J Neurosci* **29**:3103–3108

72. Spaiardi P, Tavazzani E, Manca M, Milesi V, Russo G, Prigioni I, Marcotti W, Magistretti J, Masetto S (2017) **An allosteric gating model recapitulates the biophysical properties of I K,L expressed in mouse vestibular type I hair cells: Allosteric gating of I K,L** *J Physiol* **595**:6735–6750

73. Spaiardi P, Tavazzani E, Manca M, Russo G, Prigioni I, Biella G, Giunta R, Johnson SL, Marcotti W, Masetto S (2020) **K+ Accumulation and Clearance in the Calyx Synaptic Cleft of Type I Mouse Vestibular Hair Cells** *Neuroscience* **426**:69–86

74. Spitzmaul G, Tolosa L, Winkelman BHJ, Heidenreich M, Frens MA, Chabbert C, de Zeeuw CI, Jentsch TJ (2013) **Vestibular Role of KCNQ4 and KCNQ5 K+ Channels Revealed by Mouse Models*** *Journal of Biological Chemistry* **288**:9334–9344

75. Stone JS, Pujol R, Nguyen TB, Cox BC (2021) **The Transcription Factor Sox2 Is Required to Maintain the Cell Type-Specific Properties and Innervation of Type II Vestibular Hair Cells in Adult Mice** *J Neurosci* **41**:6217–6233

76. Stühmer W, Ruppersberg JP, Schröter KH, Sakmann B, Stocker M, Giese KP, Perschke A, Baumann A, Pongs O (1989) **Molecular basis of functional diversity of voltage-gated potassium channels in mammalian brain** *EMBO J* **8**:3235–3244

77. Vollrath MA, Eatock RA (2003) **Time course and extent of mechanotransducer adaptation in mouse utricular hair cells: Comparison with frog saccular hair cells** *Journal of Neurophysiology* **90**:2676–2689

78. Wang H (1998) **KCNQ2 and KCNQ3 Potassium Channel Subunits: Molecular Correlates of the M-Channel** *Science* **282**:1890–1893

79. Wersäll J (1956) **Studies on the structure and innervation of the sensory epithelium of the cristae ampulares in the guinea pig; a light and electron microscopic investigation** *Acta Otolaryngol Suppl* **126**:1–85

80. Wong WH, Hurley KM, Eatock RA (2004) **Differences Between the Negatively Activating Potassium Conductances of Mammalian Cochlear and Vestibular Hair Cells** *J Assoc Res Otolaryngol* **5**:270–284

81. Xu T *et al.* (2007) **Roles of Alternative Splicing in the Functional Properties of Inner Ear-specific KCNQ4 Channels** *J Biol Chem* **282**:23899–23909

82. Yao X (2002) **Expression of KCNA10, a Voltage-Gated K Channel, in Glomerular Endothelium and at the Apical Membrane of the Renal Proximal Tubule** *Journal of the American Society of Nephrology* **13**:2831–2839

Editors

Reviewing Editor
Andrew King
University of Oxford, Oxford, United Kingdom

Senior Editor
Andrew King
University of Oxford, Oxford, United Kingdom

Reviewer #1 (Public Review):

Summary:

In this paper the authors provide a thorough demonstration of the role that one particular type of voltage-gated potassium channel, Kv1.8, plays in a low voltage activated conductance found in type I vestibular hair cells. Along the way, they find that this same channel protein appears to function in type II vestibular hair cells as well, contributing to other macroscopic

conductances. Overall, Kv1.8 may provide especially low input resistance and short time constants to facilitate encoding of more rapid head movements in animals that have necks. Combination with other channel proteins, in different ratios, may contribute to the diversified excitability of vestibular hair cells.

Strengths:

The experiments are comprehensive and clearly described, both in text and in the figures. Statistical analyses are provided throughout.

Weaknesses:

None.

https://doi.org/10.7554/eLife.94342.2.sa3

Reviewer #2 (Public Review):

The focus of this manuscript was to investigate whether Kv1.8 channels, which have previously been suggested to be expressed in type I hair cells of the mammalian vestibular system, are responsible for the potassium conductance gK,L. This is an important study because gK,L is known to be crucial for the function of type I hair cells, but the channel identity has been a matter of debate for the past 20 years. The authors have addressed this research topic by primarily investigating the electrophysiological properties of the vestibular hair cells from Kv1.8 knockout mice. Interestingly, gK,L was completely abolished in Kv1.8-deficient mice, in agreement with the hypothesis put forward by the authors based on the literature. The surprising observation was that in the absence of Kv1.8 potassium channels, the outward potassium current in type II hair cells was also largely reduced. Type II hair cells express the largely inactivating potassium conductance g,K,A, but not gK,L. The authors concluded that heteromultimerization of non-inactivating Kv1.8 and the inactivating Kv1.4 subunits could be responsible for the inactivating gK,A. Overall, the manuscript is very well written and most of the conclusions are supported by the experimental work. The figures are well described, and the statistical analysis is robust.

https://doi.org/10.7554/eLife.94342.2.sa2

Reviewer #3 (Public Review):

Summary:

This paper by Martin et al. describes the contribution of a Kv channel subunit (Kv1.8, KCNA10) to voltage-dependent K+ conductances and membrane properties of type I and type II hair cells of the mouse utricle. Previous work has documented striking differences in K+ conductances between vestibular hair cell types. In particular amniote type I hair cells are known to express a non-typical low-voltage-activated K+ conductance (GK,L) whose molecular identity has been elusive. K+ conductances in hair cells from 3 different mouse genotypes (wildtype, Kv1.8 homozygous knockouts and heterozygotes) are examined here and whole cell patch-clamp recordings indicate a prominent role for Kv1.8 subunits in generating GK,L. Results also interestingly support a role for Kv1.8 subunits in type II hair cell K+ conductances; inactivating conductances in null mice are reduced in type II hair cells from striola and extrastriola regions of the utricle. Kv1.8 is therefore proposed to contribute as a pore-forming subunit for 3 different K+ conductances in vestibular hair cells. The impact of these conductances on membrane responses to current steps is studied in current clamp. Pharmacological experiments use XE991 to block some residual Kv7-mediated current in both hair cell types, but no other pharmacological blockers are used. In addition immunostaining

data are presented and raise some questions about Kv7 and Kv1.8 channel localization. Overall, the data present compelling evidence that removal of Kv1.8 produces profound changes in hair cell membrane conductances and sensory capabilities. These changes at hair cell level suggest vestibular function would be compromised and further assessment in terms of balance behavior in the different mice would be interesting.

Strengths:

This study provides strong evidence that Kv1.8 subunits are major contributors to the unusual K+ conductance in type I hair cells of the utricle. It also indicates that Kv1.8 subunits are important for type II hair cell K+ conductances because Kv1.8-/- mice lacked an inactivating A conductance and had reduced delayed rectifier conductance compared to controls. A comprehensive and careful analysis of biophysical profiles is presented of expressed K+ conductances in 3 different mouse genotypes. Voltage-dependent K+ currents are rigorously characterized at a range of different ages and their impact on membrane voltage responses to current input is studied. Some pharmacological experiments are performed in addition to immunostaining to bolster the conclusions from the biophysical studies. The paper has a significant impact in showing the role of Kv1.8 in determining utricular hair cell electrophysiological phenotypes.

Weaknesses:

(1) From previous work it is known that GK,L in type I hair cells has unusual ion permeation and pharmacological properties that differ greatly from type II hair cell conductances. Notably GK,L is highly permeable to Cs+ as well as K+ ions and is slightly permeable to Na+. It is blocked by 4-aminopyridine and divalent cations (Ba2+, Ca2+, Ni2+), enhanced by external K+ and modulated by cyclic GMP. The question arises-if Kv1.8 is a major player and pore-forming subunit in type I and type II cells (and cochlear inner hair cells as shown by Dierich et al. 2020) how are subunits modified to produce channels with very different properties? A role for Kv1.4 channels (gA) is proposed in type II hair cells based on previous findings in bird hair cells. However, hair cell specific partner interactions with Kv1.8 that result in GK,L in type I hair cells and Cs+ impermeable, inactivating currents in type II hair cells remain for the most part unexplored.

(2) Data from patch-clamp and immunocytochemistry experiments are not in close alignment. XE991 (Kv7 channel blocker) decreases remaining K+ conductance in type I and type II hair cells from null mice supporting the presence of Kv7 channels in hair cells (Fig. 7). Also, Holt et al. (2007) previously showed inhibition of GK,L in type I hair cells (but not delayed rectifier conductance in type II hair cells) using a dominant negative construct of Kv7.4 channels. However, immunolabelling indicates Kv7.4 channels on the inner face of calyx terminals adjacent to hair cells (Fig. 5). Some reconciliation of these findings is needed.

(3) A previous paper reported that a vestibular evoked potential was abnormal in Kv1.8-/- mice (Lee et al. 2013) as briefly mentioned (lines 94-95). It would be really interesting to know if any vestibular-associated behaviors and/or hearing loss were observed in the mice populations. If responses are compromised at the sensory hair cell level across different zones, degradation of balance function would be anticipated and should be elucidated.

https://doi.org/10.7554/eLife.94342.2.sa1

Author response:

The following is the authors' response to the original reviews.

> ***Recommendations for the authors:***
>
> ***Reviewer #1 (Recommendations For The Authors):***
>
> *Line 127. Provide a few more words describing the voltage protocol. To the uninitiated, panels A and B will be difficult to understand. "The large negative step is used to first close all channels, then probe the activation function with a series of depolarizing steps to re-open them and obtain the max conductance from the peak tail current at -36 mV. "*

We have revised the text as suggested (revision lines 127 to Line 131): “From a holding potential within the gK,L activation range (here –74 mV), the cell is hyperpolarized to –124 mV, negative to EK and the activation range, producing a large inward current through open gK,L channels that rapidly decays as the channels deactivate. We use the large transient inward current as a hallmark of gK,L. The hyperpolarization closes all channels, and then the activation function is probed with a series of depolarizing steps, obtaining the max conductance from the peak tail current at –44 mV (Fig. 1A).”

> *Incidentally, why does the peak tail current decay?*

We added this text to the figure legend to explain this: “For steps positive to the midpoint voltage, tail currents are very large. As a result, K+ accumulation in the calyceal cleft reduces driving force on K+, causing currents to decay rapidly, as seen in A (Lim et al., 2011).”

> *The decay of the peak tail current is a feature of gK,L (large K+ conductance) and the large enclosed synaptic cleft (which concentrates K+ that effluxes from the HC). See Govindaraju et al. (2023) and Lim et al. (2011) for modeling and experiments around this phenomenon.*
>
> *Line 217-218. For some reason, I stumbled over this wording. Perhaps rearrange as "In type II HCs absence of Kv1.8 significantly increased Rin and tauRC. There was no effect on Vrest because the conductances to which Kv1.8 contributes, gA and gDR activate positive to the resting potential. (so which K conductances establish Vrest???).*

We kept our original wording because we wanted to discuss the baseline (Vrest) before describing responses to current injection.

Vrest is presumably maintained by ATP-dependent Na/K exchangers (ATP1a1), HCN, Kir, and mechanotransduction currents. Repolarization is achieved by delayed rectifier and A-type K+ conductances in type II HCs.

> *Figure 4, panel C - provides absolute membrane potential for voltage responses. Presumably, these were the most 'ringy' responses. Were they obtained at similar Vm in all cells (i.e., comparisons of Q values in lines 229-230).*

We added the absolute membrane potential scale. Type II HC protocols all started with 0 pA current injection at baseline, so they were at their natural Vrest, which did not differ by genotype or zone. Consistent with Q depending on expression of conductances that activate positive to Vrest, Q did not co-vary with Vrest (Pearson’s correlation coefficient = 0.08, p = 0.47, n= 85).

> *Lines 254. Staining is non-specific? Rather than non-selective?*

Yes, thanks - Corrected (Line 264).

> *Figure 6. Do you have a negative control image for Kv1.4 immuno? Is it surprising that this label is all over the cell, but Kv1.8 is restricted to the synaptic pole?*

We don't have a null-animal control because this immunoreactivity was done in rat. While the cuticular plate staining was most likely nonspecific because we see that with many different antibodies, it's harder to judge the background staining in the hair cell body layer. After feedback from the reviewers, we decided to pull the KV1.4 immunostaining from the paper because of the lack of null control, high background, and inability to reproduce these results in mouse tissue. In our hands, in mouse tissue, both mouse and rabbit anti-KV1.4 antibodies failed to localize to the hair cell membrane. Further optimization or another method could improve that, but for now the single-cell expression data (McInturff et al., 2018) remain the strongest evidence for KV1.4 expression in murine type II hair cells.

> *Lines 400-404. Whew, this is pretty cryptic. Expand a bit?*

We simplified this paragraph (revision lines 411-413): "We speculate that gA and gDR(KV1.8) have different subunit composition: gA may include heteromers of KV1.8 with other subunits that confer rapid inactivation, while gDR(KV1.8) may comprise homomeric KV1.8 channels, given that they do not have N-type inactivation ."

> *Line 428. 'importantly different ion channels'. I think I understand what is meant but perhaps say a bit more.*

Revised (Line 438): "biophysically distinct and functionally different ion channels".

> *Random thought. In addition to impacting Rin and TauRC, do you think the more negative Vrest might also provide a selective advantage by increasing the driving force on K entry from endolymph?*

When the calyx is perfectly intact, gK,L is predicted to make Vrest less negative than the values we report in our paper, where we have disturbed the calyx to access the hair cell (–80, Govindaraju et al., 2023, *vs.* –87 mV, here). By enhancing K+ accumulation in the calyceal cleft, the intact calyx shifts EK—and Vrest—positively (Lim et al., 2011), so the effect on driving force may not be as drastic as what you are thinking.

> ***Reviewer #2 (Recommendations For The Authors):***
>
> *(1) Introduction: wouldn't the small initial paragraph stating the main conclusion of the study fit better at the end of the background section, instead of at the beginning?*

Thank you for this idea, we have tried that and settled on this direct approach to let people know in advance what the goals of the paper are.

> *(2) Pg.4: The following sentence is rather confusing "Between P5 and P10, we detected no evidence of a non-gK,L KV1.8-dependent.....". Also, Suppl. Fig 1A seems to show that between P5 and P10 hair cells can display a potassium current having either a hyperpolarised or depolarised Vhalf. Thus, I am not sure I understand the above statement.*

Thank you for pointing out unclear wording. We used the more common "delayed rectifier" term in our revision (Lines 144-147): "Between P5 and P10, some type I HCs have not yet acquired the physiologically defined conductance, gK,L.. N effects of KV1.8 deletion were seen

in the delayed rectifier currents of immature type I HCs (Suppl. Fig. 1B), showing that they are not immature forms of the Kv1.8-dependent gK,L channels. ”

> *(3) For the reduced Cm of hair cells from Kv1.8 knockout mice, could another reason be simply the immature state of the hair cells (i.e. lack of normal growth), rather than less channels in the membrane?*

There were no other signs to suggest immaturity or abnormal growth in KV1.8–/– hair cells or mice. Importantly, type II HCs did not show the same Cm effect.

We further discussed the capacitance effect in lines 160-167: “Cm scales with surface area, but soma sizes were unchanged by deletion of KV1.8 (Suppl. Table 2). Instead, Cm may be higher in KV1.8+/+ cells because of gK,L for two reasons. First, highly expressed trans-membrane proteins (see discussion of gK,L channel density in Chen and Eatock, 2000) can affect membrane thickness (Mitra et al., 2004), which is inversely proportional to specific Cm. Second, gK,L could contaminate estimations of capacitive current, which is calculated from the decay time constant of transient current evoked by small voltage steps *outside* the operating range of any ion channels. gK,L has such a negative operating range that, even for Vm negative to –90 mV, some gK,L channels are voltage-sensitive and could add to capacitive current.”

> *(4) Methods: The electrophysiological part states that "For most recordings, we used .....". However, it is not clear what has been used for the other recordings.*

Thanks for catching this error, a holdover from an earlier ms. version. We have deleted “For most recordings” (revision line 466).

Also, please provide the sign for the calculated 4 mV liquid junction potential.

Done (revision line 476).

> ***Reviewer #3 (Recommendations For The Authors):***
>
> ***(****1) Some of the data in panels in Fig. 1 are hard to match up. The voltage protocols shown in A and B show steps from hyperpolarized values to -71mV (A) and -32 mV (B). However, the value from A doesn't seem to correspond with the activation curve in C.*

Thank you for catching this. We accidentally showed the control I-X curve from a different cell than that in A. We now show the G-V relation for the cell in A.

> *Also the Vhalf in D for -/- animals is ~-38 mV, which is similar to the most positive step shown in the protocol.*

The most positive step in Figure 1B is actually –25 mV. The uneven tick labels might have been confusing, so we re-labeled them to be more conventional.

> *Were type I cells stepped to more positive potentials to test for the presence of voltage-activated currents at greater depolarizations? This is needed to support the statement on lines 147-148.*

We added “no additional K+ conductance activated up to +40 mV” (revision line 149-150). Our standard voltage-clamp protocol iterates up to ~+40 mV in KV1.8–/– hair cells, but in Figure 1 we only showed steps up to –25 mV because K+ accumulation in the synaptic cleft with the calyx distorts the current waveform even for the small residual conductances of the knockouts. KV1.8–/– hair cells have a main KV conductance with a Vhalf of ~–38 mV, as shown

in Figure 1, and we did not see an additional KV conductance that activated with a more positive Vhalf up to +40 mV.

> *(2) Line 151 states "While the cells of Kv1.8-/- appeared healthy..." how were epithelia assessed for health? Hair cells arise from support cells and it would be interesting to know if Kv1.8 absence influences supporting cells or neurons.*

We added our criteria for cell health to lines 477-479: “KV1.8–/– hair cells appeared healthy in that cells had resting potentials negative to –50 mV, cells lasted a long time (20-30 minutes) in ruptured patch recordings, membranes were not fragile, and extensive blebbing was not seen.”

Supporting cells were not routinely investigated. We characterized calyx electrical activity (passive membrane properties, voltage-gated currents, firing pattern) and didn’t detect differences between +/+, +/–, and –/– recordings (data not shown). KV1.8 was not detected in neural tissue (Lee et al., 2013).

> *(3) Several different K+ channel subtypes were found to contribute to inner hair cell K+ conductances (Dierich et al. 2020) but few additional K+ channel subtypes are considered here in vestibular hair cells. Further comments on calcium-activated conductances (lines 310-317) would be helpful since apamin-sensitive SK conductances are reported in type II hair cells (Poppi et al. 2018) and large iberiotoxin-sensitive BK conductances in type I hair cells (Contini et al. 2020). Were iberiotoxin effects studied at a range of voltages and might calcium-dependent conductances contribute to the enhanced resonance responses shown in Fig. 4?*

We refer you to lines 310-317 in the original ms (lines 322-329 in the revised ms), where we explain possible reasons for not observing IK(Ca) in this study.

> *(4) Similar to GK,L erg (Kv11) channels show significant Cs+-permeability. Were experiments using Cs+ and/or Kv11 antagonists performed to test for Kv11?*

No. Hurley et al. (2006) used Kv11 antagonists to reveal Kv11 currents in rat utricular type I hair cells with perforated patch, which were also detected in rats with single-cell RT-PCR (Hurley et al. 2006) and in mice with single-cell RNAseq (McInturff et al., 2018). They likely contribute to hair cell currents, alongside Kv7, Kv1.8, HCN1, and Kir.

> *(5) Mechanosensitive ("MET") channels in hair cells are mentioned on lines 234 and 472 (towards the end of the Discussion), but a sentence or two describing the sensory function of hair cells in terms of MET channels and K+ fluxes would help in the Introduction too.*

Following this suggestion we have expanded the introduction with the following lines (78-87): “Hair cells are known for their large outwardly rectifying K+ conductances, which repolarize membrane voltage following a mechanically evoked perturbation and in some cases contribute to sharp electrical tuning of the hair cell membrane. Because gK,L is unusually large and unusually negatively activated, it strongly attenuates and speeds up the receptor potentials of type I HCs (Correia et al., 1996; Rüsch and Eatock, 1996b). In addition, gK,L augments a novel non-quantal transmission from type I hair cell to afferent calyx by providing open channels for K+ flow into the synaptic cleft (Contini et al., 2012, 2017, 2020; Govindaraju et al., 2023), increasing the speed and linearity of the transmitted signal (Songer and Eatock, 2013).”

> *(6) Lines 258-260 state that GKL does not inactivate, but previous literature has documented a slow type of inactivation in mouse crista and utricle type I hair cells (Lim et al. 2011, Rusch and Eatock 1996) which should be considered.*

Lim et al. (2011) concluded that K+ accumulation in the synaptic cleft can explain much of the apparent inactivation of gK,L. In our paper, we were referring to fast, N-type inactivation. We changed that line to be more specific; new revision lines 269-271: "KV1.8, like most KV1 subunits, does not show fast inactivation as a heterologously expressed homomer (Lang et al., 2000; Ranjan et al., 2019; Dierich et al., 2020), nor do the KV1.8-dependent channels in type I HCs, as we show, and in cochlear inner hair cells (Dierich et al., 2020)."

> *(7) Lines 320-321 Zonal differences in inward rectifier conductances were reported previously in bird hair cells (Masetto and Correia 1997) and should be referenced here.*

Zonal differences were reported by Masetto and Correia for type II but not type I avian hair cells, which is why we emphasize that we found a zonal difference in I-H in type I hair cells. We added two citations to direct readers to type II hair cell results (lines 333-334): "The gK,L knockout allowed identification of zonal differences in IH and IKir in type I HCs, previously examined in type II HCs (Masetto and Correia, 1997; Levin and Holt, 2012)."

> *Also, Horwitz et al. (2011) showed HCN channels in utricles are needed for normal balance function, so please include this reference (see line 171).*

Done (line 184).

> *(8) Fig 6A. Shows Kv1.4 staining in rat utricle but procedures for rat experiments are not described. These should be added. Also, indicate striola or extrastriola regions (if known).*

We removed KV1.4 immunostaining from the paper, see above.

> *(9) Table 6, ZD7288 is listed -was this reagent used in experiments to block Gh? If not please omit.*

ZD7288 was used to block gH to produce a clean h-infinity curve in Figure 6, which is described in the legend.

> *(10) In supplementary Fig. 5A make clear if the currents are from XE991 subtraction. Also, is the G-V data for single cell or multiple cells in B? It appears to be from 1 cell but ages P11-505 are given in legend.*

The G-V curve in B is from XE991 subtraction, and average parameters in the figure caption are for all the KV1.8–/– striolar type I hair cells where we observed this double Boltzmann tail G-V curve. I added detail to the figure caption to explain this better.

> *(11) Supplementary Fig. 6A claims a fast activation of inward rectifier K+ channels in type II but not type I cells-not clear what exactly is measured here.*

We use "fast inward rectifier" to indicate the inward current that increases within the first 20 ms after hyperpolarization from rest (IKir, characterized in Levin & Holt, 2012) in contrast to HCN channels, which open over ~100 ms. We added panel C to show that the activation of IKir is visible in type II hair cells but not in the knockout type I hair cells that lack gK,L. IKir was a reliable cue to distinguish type I and type II hair cells in the knockout.

For our actual measurements in Fig 6B, we quantified the current flowing after 250 ms at –124 mV because we did not pharmacologically separate IKir and IH.

> *Could the XE991-sensitive current be activated and contributing?*

The XE991-sensitive current could decay (rapidly) at the onset of the hyperpolarizing step, but was not contributing to our measurement of IKir and IH, made after 250 ms at –124 mV, at which point any low-voltage-activated (LVA) outward rectifiers have deactivated. Additionally, the LVA XE991-sensitive currents were rare (only detected in some striolar type I hair cells) and when present did not compete with fast IKir, which is only found in type II hair cells.

> *Also, did the inward rectifier conductances sustain any outward conductance at more depolarized voltage steps?*

For the KV1.8-null mice specifically, we cannot answer the question because we did not use specific blocking agents for inward rectifiers. However, we expect that there would only be sustained outward IR currents at voltages between EK and ~-60 mV: the foot of IKir's I-V relation according to published data from mouse utricular hair cells – e.g., Holt and Eatock 1995, Rusch and Eatock 1996, Rusch et al. 1998, Horwitz et al., 2011, etc. Thus, any such current would be unlikely to contaminate the residual outward rectifiers in Kv1.8-null animals, which activate positive to ~-60 mV.

(I-HCN is also not a problem, because it could only be outward positive to its reversal potential at ~-40 mV, which is significantly positive to its voltage activation range.)

https://doi.org/10.7554/eLife.94342.2.sa0